UNCLASSIFIED

AD 290 058

Reproduced by the

ARMED SERVICES TECHNICAL INFORMATION AGENOW ARLINGTON HALL STATION ARLINGTON 12, VIRGINIA



UNCLASSIFIED

NOTICE: When government or other drawings, specifications or other data are used for any purpose other than in connection with a definitely related government procurement operation, the U. S. Government thereby incurs no responsibility, nor any obligation whatsoever; and the fact that the Government may have formulated, furnished, or in any way supplied the said drawings, specifications, or other data is not to be regarded by implication or otherwise as in any manner licensing the holder or any other person or corporation, or conveying any rights or permission to manufacture, use or sell any patented invention that may in any way be related thereto.

CATALOGEN DA TOTTA AS AD NO 290 058

290 058



HUGHES TOOL COMPANY · AIRCRAFT DIVISION

Culver City, California

Contract No. AF 33(600)-30271

Report 285-9-7 (61-79)

HOT CYCLE ROTOR SYSTEM

RESULTS OF STATIC TEST PROGRAM
GAS FLOWS AND TEMPERATURES

February 1962 Revised June 1962

HUGHES TOOL COMPANY -- AIRCRAFT DIVISION

Culver City, California

For

Commander

Aeronautical Systems Division

Prepared by:

D. L. Jones Head, Propulsion Group

J. W. Rabek Aerodynamics Specialist

Approved by: Kodney A.

R. A. Boudreaux

Chief, Aerodynamics

Section

J. L. Velazquez

Sr. Project Engineer

H. O. Nav

Manager, Transport

Helicopter

FOREWORD

This report has been prepared by Hughes Tool Company - Aircraft Division under USAF Contract AF 33(600)-30271 "Hot Cycle Pressure Jet Rotor System", D/A Project Number 9-38-01-000, Subtask 616.

The Hot Cycle Pressure Jet Rotor System is based on a principle wherein the exhaust gases from high pressure ratio turbojet engine(s) located in the fuselage are ducted through the rotor hub and blades and are exhausted through a nozzle at the blade tip. Forces thus produced drive the rotor.

Summarized herein are the analyses and tests relating to determination of duct losses, nozzle coefficients and similar data used in analyzing the efficiencies of the Hot Cycle System. This report is in partial fulfillment of Item 6C, covering Component and Assembly Tests performed under Item 6a (4) and 7a of the contract.

ABSTRACT

This report provides an aerothermal survey (test and analysis) of the Hot Cycle whirl test system under static conditions and includes a tether test, hub cooling test, and J57 gas generator calibration. Emphasis is placed on correlation of test data with earlier derived values used in performance predictions. In general, agreement between predicted and measured values of duct losses, nozzle coefficients and tip thrust was realized. Most significant, the tip nozzle effective velocity coefficient, directly proportional to tip thrust, was measured to be 0.98, 2.5% better than predicted. Hub cooling is shown to be satisfactory and no overtemperaturing of hub or spar components has been encountered. The normal engine operating line, including turbine discharge pressure and temperature versus high pressure compressor rpm, has been established. Also, exhaust valve controlled "off-line" turbine discharge temperatures have proven to be sufficient to meet contractual requirements.

	TABLE OF CONTENTS	Page									
1.	Introduction	1									
2.	Primary Duct Pressure Loss Characteristics										
3•	Rotor Tip Thrust										
4.	Nozzle Parameters										
5.	Hub Cooling Path Flow Characteristics										
6.	Gas Generator Installation and Operating Characteristics	26									
	6.1 Installation	26									
	6.2 Initial Operation and Calibration	28									
	6.3 System Tests	36									
7.	Summary										
8.	References	39									
9•	Nomenclature	40									
	9.1 Symbols	40									
	9.2 Superscripts	42									
	9.3 Subscripts	42									
10.	Appendix I; Flow Data Analysis	44									
	10.1 Flow Measurement	44									
	10.2 Mass Weighted Nozzle Inlet Total Pressure	63									
11.	Appendix II; Derivation of Nozzle Coefficients	65									
	11.1 Effective Velocity Coefficient	65									
	11.2 Thrust Coefficient	67									
	11.3 Flow Coefficient	69									

LIST OF FIGURES

	HUGHES TOOL (COMPAN
	TTOM OF TTOWNS	•
	LIST OF FIGURES	Page
1.	Hot Cycle Helicopter Whirl Test Installation	2
2,a	Internal View of Control Van, Engine Rotor Controls	3
2,6	Internal View of Control Van; Temperature, Pressure, and Strain Recording Instruments	4
3•	Primary Flow Path Through Hub	6
4.	Thrust Test Blade in Tethered Position	9
5.	Comparison of Rotor Tip Thrust as a Function of Turbine Discharge Pressure with and without Nozzle Probes Installed	12
6.	Nozzle Inlet Station Temperature and Pressure Probes Temporarily Installed for Tether Test	14
7,a	Nozzle Effective Velocity Coefficient vs Flow Weighted Mean Nozzle Pressure Ratio	17
7,b	Nozzle Thrust Coefficient vs Flow Weighted Mean Nozzle Pressure Ratio	18
7,c	Nozzle Flow Coefficient vs Flow Weighted Mean Nozzle Pressure Ratio	19
8.	Cooling Flow Circuit through Hub and Blade Root	21
9•	Typical Flexible Couplings Attached to Blades for Tether Operation and Hub Cooling Calibration	22
10.	Hub Cooling Blower Arrangement	23
11.	Hub Circuit, Corrected Cooling Flow vs Corrected Rotor Tip Speed	25
12,a	J57 Gas Generator Installation	. 27
12,b	Auxiliary Power and Cooling Units for Whirl Test Installation	2 9
13.	J57 Engine in Calibration Position	30
14.	Turbine Discharge Temperature vs High Pressure Compressor $\%$ rpm for J57	31
15.	Turbine Discharge Pressure vs High Pressure Compressor % rpm for J57	32
16.	Fuel Flow Rate vs High Pressure Compressor % rpm for J57	33
17.	Effect of Humidity on Corrected Fuel Flow	34

LIST OF FIGURES (Continued)

	HUGHES TOOL COM	MPANY (M)
		↑
	LIST OF FIGURES (Continued)	35 37 45
18.	J57-P-19W On and Off-Line Comparison with the T64	35 P
19.	Comparison of Streamwise Temperature Measurements	37
20.	Velocity Profiles in Branch II	45 07
21.	Permanent Streamwise Flow and Pressure Measuring Stations	46
22.	Velocity Distribution in Circular Tubes	53
23.	Variation of Average Axial Velocity with Reynolds Number for Flow in Smooth Circular Tubes.	54
24.	Gas Constant vs Water Content for C $_{n}^{H}$ (similar to JP-4) Combustion Product - Water Vapor Mixtures for Several Values of Fuel - Air Combustion Ratios.	55
25 , a	Ratio of Specific Heats for C_nH_{2n} Combustion Product - Water Vapor Mixtures vs Temperature; 0 to 12 % water; Stiochiometric Fuel - Air Ratio	56
25,ъ	Ratio of Specific Heats for C _n H _{2n} Combustion Product - Water Vapor Mixtures vs Temperature; O to 12% Water; 200% Theoretical Air	57
25,c	Ratio of Specific Heats for C_nH_{2n} Combustion Product - Water Vapor Mixtures vs Temperature; 0 to 12% water; 400% Theoretical Air	58
25,đ	Ratio of Specific Heats for C_nH_{2n} Combustion Product - Water Vapor Mixtures vs Temperature; 0 to 12% Water; 600% Theoretical Air	59
25 , e	Ratio of Specific Heats for C_nH_{2n} Combustion Product - Water Vapor Mixture vs T_e mperature; 0 to 12% Water; 800% Theoretical Air	60
26.	Atmospheric Water Content at Sea Level	61
27.	Water Injection Flow Meter Calibration	62
28.	Station Designations for Nozzle Coefficient	66

LIST OF TABLES

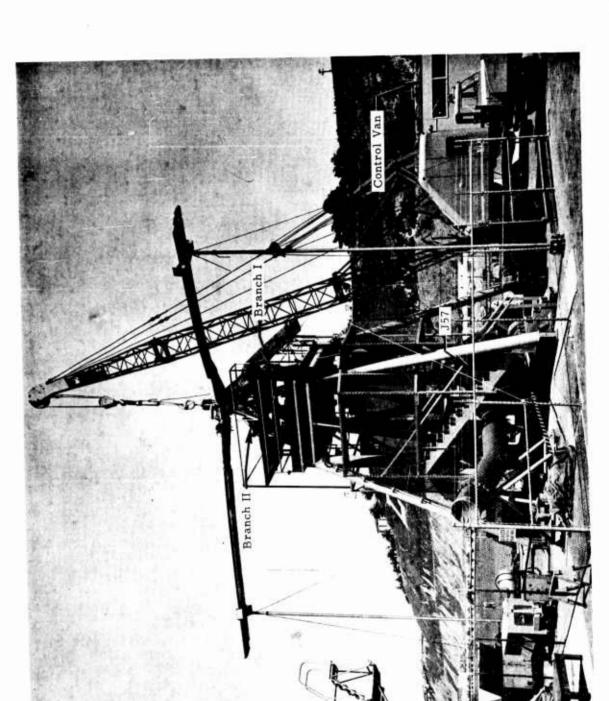
		Page	F
1.	Tether Test Streamwise Pressure and Pressure Loss Characteristics	7	P
2.	Tip Nozzle Thrust and Flow Data for Tether Test	11	Ť
3•	J57 Engine and Flow Parameters for Tether Test	7 - 51	5 0



INTRODUCTION

The Hot Cycle Helicopter whirl test installation is shown in Figure 1 and internal views of the control van are presented in Figure 2. To determine the thrust, pressure loss, and temperature characteristics of the primary and secondary flow circuits of the rotor system, as well as the effect of exhaust dump valve position on the Pratt and Whitney J57 engine's performance, a number of tests were performed as follows:

- Tether Test The rotor was attached to a fixed jig by a cable on which a tension load cell was attached. Flow was allowed in one blade only by sealing the remaining two. Calibrated strains in the load cell then permitted a direct measurement of the thrust of one blade. This electro-mechanical measurement coupled with flow, pressure, and temperature measurements provided the required data to determine tip nozzle coefficients. The flow measurements allowed a check on the suitability of the provided flow instrumentation and the pressure and temperature measurements gave a check on pressure and temperature losses in some duct components.
- Hub Cooling Circuit Calibration With the blades non-rotating, ducts were attached to the exhaust ports of the hub cooling circuit to simulate the centrifugally pumped cooling air by artificial suction. Through this simulation, the hub cooling circuit was calibrated to determine whether the cooling passages were appropriately sized.
- J57 Engine Performance With the vertical duct valve closed, the J57 was operated at military power with the exhaust dump valve in a number of positions to determine the effect of this latter valve on the J57's exhaust temperature and pressure. This was done in order to ascertain whether the



Report 285-9-7 (61-79)

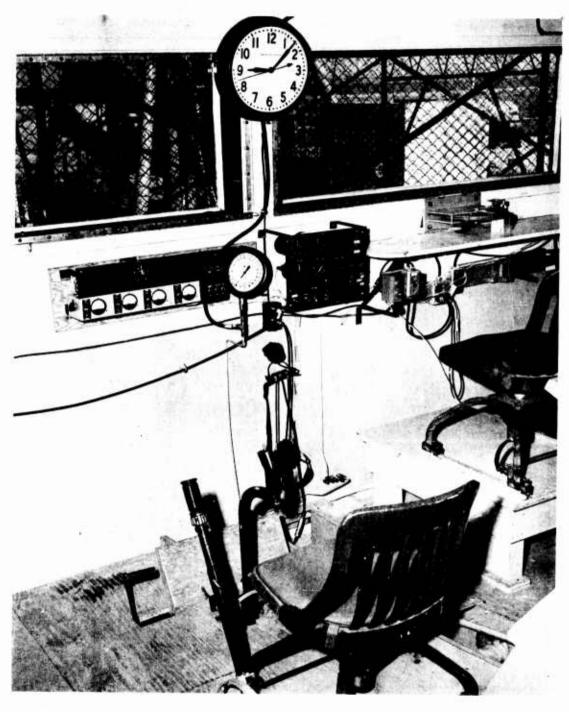
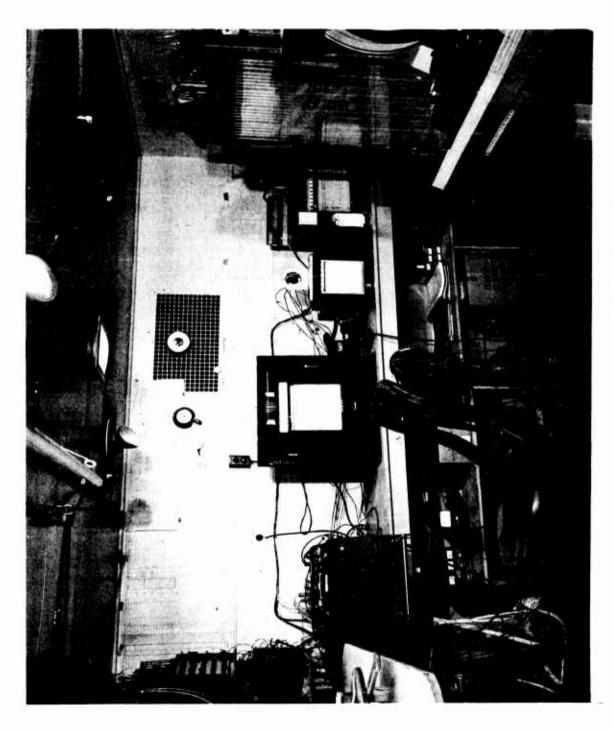


Figure 2, a. Internal View of Control Van Engine and Rotor Controls



Report 285-9-7 (61-79)

J57 could suitably approximate the exhaust conditions of the Hot Cycle design (based on the General Electric T64 engine) by operation nearer to the J57 stall line.

This report provides test results and accompanying analyses to determine the "as built" aerothermal parameters of the hot cycle system. Discussed also, is the connection of these parameters to test conditions studied and to setup limitations.



2. PRIMARY DUCT PRESSURE LOSS CHARACTERISTICS

The tether test data of Sections 3 and 4 provide pressure losses of the primary flow system. Total pressure was measured at the following stations:

- a. Ambient (Po)
- b. Turbine discharge (Pt7)
- c. Flow measuring stations in Branches I and II $(P_{tfs})_{I \text{ and } II}$
- d. Hub; below rotating seal in each branch (Pthub) I and II
- one blade (Ptnozz) LE and TE e. Nozzle inlet in each duct of

From Table 3, comparison of Columns 16 and 17 or 19 and 20 shows that the flow rates in the two stack branches are approximately 3:1 (Branch II: Branch I). This is due to the relative position of the tested blade to the whirl stand. The two stack ducts join at the hub to provide a flow cross section which is an annulus split into two 1800 segments (Figure 3). The three blades join at the hul and form an annular flow cross section which is divided into three 1200 segments. These two sets of segments are coupled at the rotating seal and had a relative position of blades to the stand (stack ducts) as in Figure 3 thereby favoring flow from Branch II.

Table I provides the loss characteristics of the ducts for the first nine runs of the tether test runs for which all instruments were installed and operating. Although the value of R, \forall , streamwise temperature ratios and mixing losses are not constant for each of these runs due to variable water injection, the pressure loss ratios ($\frac{\Delta PT}{P_m}$) are quite uniform. The pressure loss from the turbine discharge plane (Pt7) to the hub stations is of the order of 6 to 7%. This is in good agreement with previous estimates although the flow for the tether test was to one blade instead of three. Agreement was found in spite of the apparent discrepancy in flow rates between design

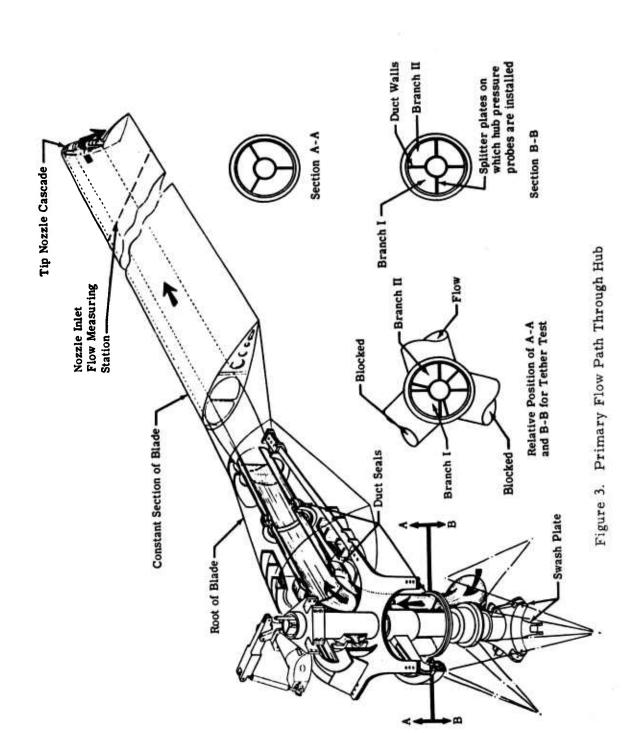


TABLE 1

Tether Test Streamwise Pressure and Pressure Loss Charecteristics

	딘										
ħ	Pt -Pt Bozz	Pt.	0.1442	95η1.0	0.1669	0.1920	0.1724	0.1764	0.1819	0.1740	0.1768
ដ	Pt -Pt nozz LE	τ. -7	0.1630	0.1724	c.1849	0.1935	c.1983	0.1990	0.2019	9961.0	9661.0
ង	Pt_T-PthubII	th.	0.070	0.0657	0.0713	0.0654	6010.0	0.0714	0.0732	0.0670	0.070
п	Pt_PthubI	44	0.0554	0.0480	0.0533	0.0461	c.0523	0.053	0.0550	0.0444	0.0516
ន	Pt-PtfsII	$^{Pt_{7}}$	6.0579	0.0512	0.0567	9670.0	0.0559	0.0565	0.0581	0.0483	9450.0
6	Pt7-PtfsI	Pt	0.0554	0340.0	0.0533	o.0461	0.0523	0.0529	0.0550	भगग्न-०	0.0512
ω	Ptnozz _{TE}	psfa	2736	291:0	3144	3221:	3481	3740	3971	1093	103
۲	Pt nozz _{LE}	psfa	2676	2861	3076	3218	3372	3646	3874	3980	3989
9	Pt nub II	psfa	2372	3230	3505	3729	3908	1221	6644	h623	14630
r.	Pt hub I										
æ	PtfsII	psfa	3012	3280	3560	37.32	3971	\$552	4572	4715	517.7
er:	Ptfs	psfa	3050	3831	3573	3806	3986	1,311	1854	4735	4729
N	* <u>*</u> -	psfa	3197	3457	3774	3330	\$20E	4552	1654	\$952	†86 †
-	P _O	psfa	71.15	2118	2118	2115	2118	2118	2118	2118	2118
		•	Н	N	m	#I	Ŋ	9	7	လ	0/

* All total pressure values in this table are averages.

and test because the flow through one branch was three times as great as the other as explained earlier. Future whirl test data will provide more realistic flow rates and a closer check on predictions.

A comparison of Columns 9 and 11 (Table 1) indicates virtually no pressure loss between the flow measuring and hub stations of Branch I. This is caused by the low flow rates in that branch yielding pressure differentials below the accuracy of the instrumentation. The losses between the hub station and the nozzle inlet plane are of the order of 14% $P_{ extstyle ext$ minus average of 11 and 12), somewhat higher than the 10 to 12% expected for flow to three static blades. This is due to diverting the flow to one blade (area and direction change from design), and to the relative position of the tested blade and whirl stand as described earlier.



3. ROTOR TIP THRUST

Rotor tip thrust was measured as a function of turbine discharge pressure and corresponding engine operating line temperatures up to 770°F without water injection for cooling. For higher pressures resulting in higher turbine discharge temperatures, water injection was employed to maintain blade temperatures below 800°F.

Blooking the flow to two of the three blades enabled a study of the tip thrust characteristics of a single blade. Although compromises, such as one feeder stack being under-fed, and high hub pressure losses resulted, the utilization of a single blade simplified the artificial skin cooling requirements (water spray) and effectively reduced the data analysis to one-third.

The tested blade was tethered as in Figure 4, the tension load cell being 90° to the blade at Station 320R. Nozzle instrumentation as discussed in Section 4 was installed for Runs 1 through 22 of Table 2 and were removed for Runs 23 through 27 to determine whether the instrument leads, having been directed through the cascade, had affected the thrust. Pertinent thrust and flow data is included in that table.

A comparison of the instrument blookage effect on rotor thrust as a function of turbine discharge pressure is presented in Figure 5. In the choked range, the uninstrumented runs provide approximately 4% more thrust.

The maximum thrust recorded was 702 lb. per blade. This value, in presence of the amplified duct losses, is lower than the maximum predicted for normal flow conditions, but compares quite favorably with the thrust computed assuming similar temperature and pressure ratio.

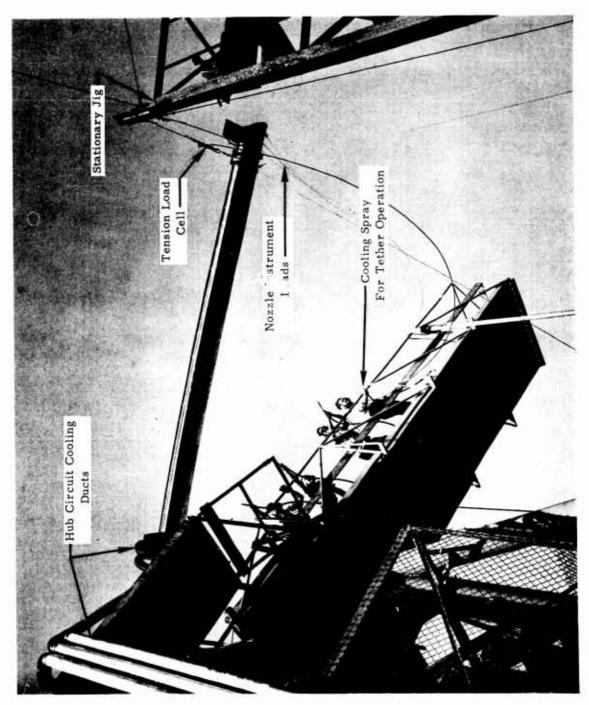


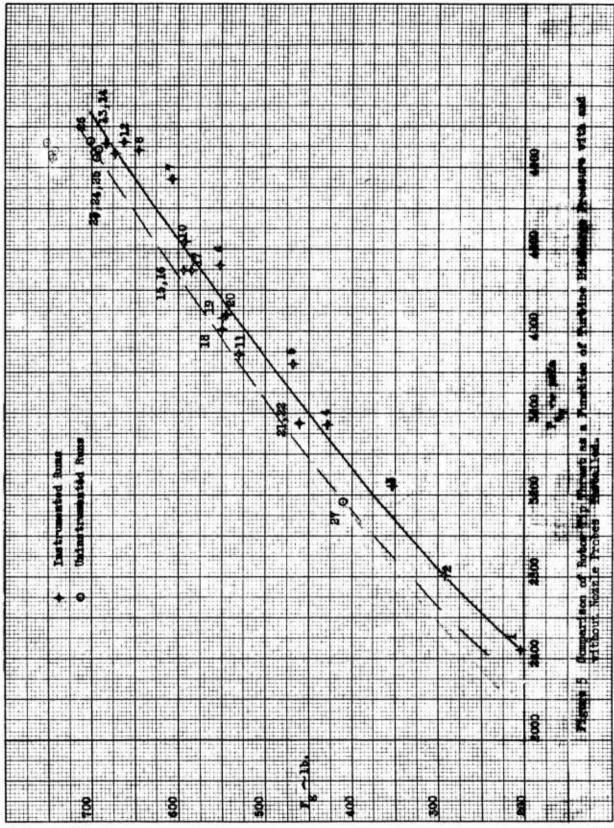
Figure 4. Thrust Tested Blade in Tethered Position



TIP NOZZLE THRUST AND FLOW DATA FOR TETHER TEST

					Lea	ding Edge Duct	Tra					
1	2	3	4	5	6	7	8	9	10	11	12	13
Run	$P_{\mathbf{t_7}}$	T _t 7	$\mathbf{P_{t}}_{\mathtt{Hub}}$	T _t fs	Pt max nozz	$\mathbf{T_{t}}_{\mathbf{nozz}}$	Wnozz	Pt max nozz	$\mathbf{T_{t_{nozz}}}$	Wozz	, # H20	Fg
#	psia	oF	psia	$\circ_{\mathbf{F}}$	ps ia	$\circ_{\mathbf{F}}$	#/sec	psia	oF	#/sec	#/sec	#
123456789101121345617890122345667	32.19 29.44 34.38 34.58 31.49 31.49 31.49 31.49 31.49 31.49 31.49 31.49 31.49 31.49 31.49 31.49 31.49 31.49 31.49	1025	20.81 22.64 24.57 26.16 27.41 29.54 31.55 32.49 32.53 32.47 32.63 32.32 32.22	558 632 720 770 605 602 608 610 690 757 805	18.86 20.29 22.85 23.95 25.87 26.38 28.37 26.58 26.58 26.58 24.47 24.56 24.47 24.56 24.40 **	558 630 720 770 600 600 608 612 690 675 730 775 720 690 765 675 710	4.06 4.46 3.38 6.52 6.55 7.49 7.20	19.33 20.28 20.28 23.63 24.74 26.60 28.15 26.89 23.94 27.81 27.85 25.54 25.25 25.25 25.28 23.28	558 635 720 770 610 605 608 608 660 665 690 665 780 755 720 680 765 675 710	4.42 4.83 5.07 5.13 6.93 7.63 7.43	0 0 0 0 1.02 1.08 1.11 1.26 1.08 1.00 0.98 1.00 0.99 ## ## ## 0.99 1.30 1.125 0	607 646 593 6684 593 6684 593 593 593 593 593 593 593 593 593 593

- * The subscript fs. pertains to the flow measuring station where $T_{tfs} \approx T_{thub}$ (mass weighted). Note that the values of Columns 7 and 10 are sometimes greater than 5, indicating blade temperature losses smaller than instrument accuracy.
- ** Nozzle instrumentation removed for these runs.
- *** Static pressure probe began to leak and provided erroneous data.
- t Max. corresponds to maximum velocity at duct center.
- W_{H_2O} total cooling water injection rate. This value is included in the sum of 8 and 11.
- ## Water flow rates were below calibration reliability (0.98 #/sec) of the flow meter.



Report 285-9-7 (61-79)



NOZZLE PARAMETERS

The tether test partially described in Section 3 provided data to establish nozzle coefficients, thereby allowing a check on previous estimates. Pressure and temperature instrumentation $(P_{t}, P \text{ and } T_{t})$ was provided in the leading and trailing edge primary flow ducts of the blade tested (Figure 6). The position of these instruments was 2 to 3 hydraulic diameters upstream of the nozzle inlet and it is assumed herein that the loss in total pressure and temperature was negligible between the plane of measurement and the nozzle inlet.

Total pressure probes were centered in each duct to establish the maximum velocity head, and the method established in Section 10 was used to determine flow rate and mass - weighted nozzle inlet total pressure. The center of pressure for the nozzle exhaust was estimated to be at Station 329.5 R.

Only a few test runs provided adequate data required to determine nozzle parameters. For the reason described in Section 3, nozzle instrumentation was installed for Runs 1 through 22 and was removed for Runs 23 - 27. During Run 10, the leading edge duct nozzle inlet static pressure probe began leaking. Runs were continued at high turbine discharge pressure values since for nozzle choked conditions, a knowledge of nozzle inlet total pressure and a previous fix on nozzle inlet Mach number establishes the flow rate when changed R, X, and area effects are negligible. During the analysis, for Runs 10 through 24 and 27 it was found that although the total pressure at the center of the duct indicated a nozzle pressure ratio above the choked value in many cases, the mass weighted mean total pressure was inadequate for choking in any of these runs. The unchoked condition then does not provide a constant nozzle inlet Mach number and thus the Pt nozz insufficient to determine flow rate. It was found that the low total pressure values at the nozzle were due to high duct losses as explained in Section 2.

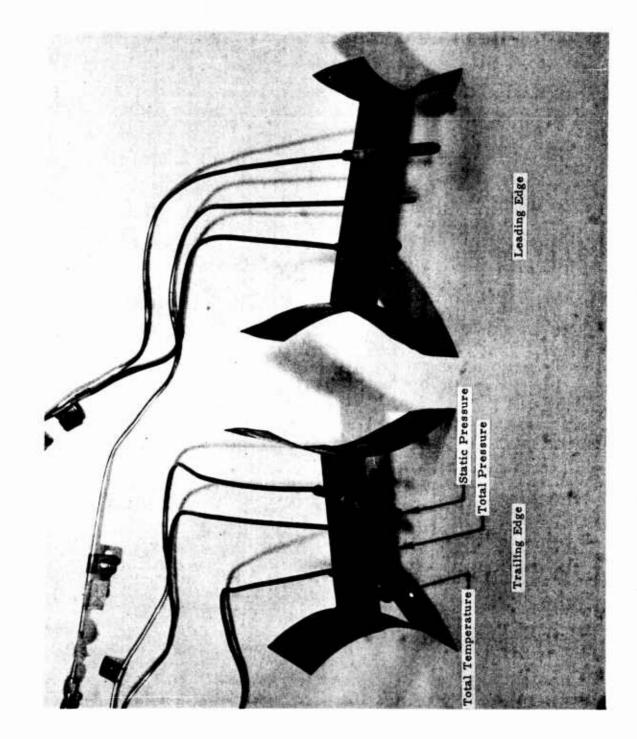


Figure 6. Nozzle Inlet Station Temperature and Pressure Probes Temporarily

by the values determined at tion 10. The flow rates decrease estimate the blade flow unchoked nozzle conditions, A second check on the flow rates is afforded by the values determined at the stack flow measuring stations discussed in Section 10. The flow rates determined from these stations could have been used to estimate the blade flow rates but since Runs 10 through 24 plus 27 provided unchoked nozzle conditions, it was decided that the results of data analysis of these runs would not significantly add to the over-all picture. However, an attempt to use flow measuring station data was made in order to establish the nozzle coefficients for the choked runs (25 and 26). The effective velocity coefficients resulting were unbelievably high and are thus not presented. This discrepancy is attributed to the effect of nozzle area change (instrument lead removal) on estimated inlet Mach number.

For the previous runs (1 through 9), there were seven unchoked and two choked cases for which redundant data at the flow measuring and nozzle inlet stations were taken. This, then, provides flow data measured at stations in series and establishes the adequacy of using Nikuradse's data (Reference 1) to measure the flow at the two parallel stack flow measuring stations as accomplished in Section 10. Except for Run 3 (Table 3, Column 34) which indicated an error of + 18.6% between the flow station measured rates and nozzle inlet station measured rates, the maximum flow measurement error for the other runs was

% error = Flow Meas. Stat. Flow - Nozz. Stat. Flow X 100 = 10.8% while for the two instrumented choked runs the maximum error was + 2.4% (based on 1st iteration, see Section 10.1).

In order to correlate the data to provide the coefficient corrections due to instrument blockage a plot of thrust with and without instrumentation must be analyzed. A study of Figure 5 indicates that in the choked region,

the thrust increase without blockage was approximately 25 lbs. The percentage of thrust increase varies from about 4% in the choked region to more than 20% at low turbine discharge pressure. Since instrumented and uninstrumented runs are compared on the plot at identical gas generator and duct conditions, the increase in gross thrust (ΔF_g) in terms of percent corresponds to identical increase in thrust coefficient (ΔC_f) . In this manner the relation between thrust coefficient as a function of NPR for uninstrumented runs can be established as shown in Figure 7b. To determine velocity and flow coefficients in similar terms a relation from Section 11 is used:

$$C_{f} = C_{vf} \times C_{w} . \tag{1}$$

and

$$(C_f + \Delta C_f) = (C_{vf} + \Delta C_{vf}) (C_w + \Delta C_w). \tag{2}$$

It is seen that the percentage effect of Δ C_f caused by C_{vf} and Δ C_w can be found only if the relationships between Δ C_{vf} and Δ C_w are known. The data taken during the tether test does not provide this relationship. However, since the change in flow coefficient (Δ C_w) is directly affected by the flow rate while the effective velocity coefficient is affected by the square root of the flow rate, only slight error is involved when assuming

$$\Delta C_{\mathbf{w}} = 2 \Delta C_{\mathbf{vf}}$$
 (3)

Equation (3), then, provides the additional relationship enabling a solution of Equation (2). However, the function of $C_{\rm vf}$ vs NPR for uninstrumented runs can be determined in two slightly different ways. First, by correcting the second iteration at one point in the choked region where the function $C_{\rm vf}$ is almost constant, and, completing the curve graphically using the existing

plot as a guide. For this purpose, in the following calculations the choke point at NPR = 1.86, was selected.

The other solution is obtained by applying Equations (2) and (3) over the entire range of NPR. The redundant plot can serve as means of checking the relationship between all three parameters. Originally, the first approach was used to establish the velocity coefficient (recommended) on Figure 7a, then from Equation (1) C (recommended) was determined on Figure 7c. Comparing the two figures it can be seen that $\Delta C_w = 2\Delta C_{vf}$ which means that the results from two methods coincide with good accuracy. Incidentally the recommended velocity coefficient C_{vf} is in close agreement with the results of many investigations made in this field. Generally, the velocity coefficient is not much affected by different nozzle shapes, methods of contraction or changes in convergence angle.

Following the first approach at NPR = 1.86, from Figure 7a, 7b and 7c at NPR = 1.86

$$C_r = 0.888, \Delta C_r = 0.031$$

$$C_{vf} = 0.968$$

$$C_{w} = 0.919$$

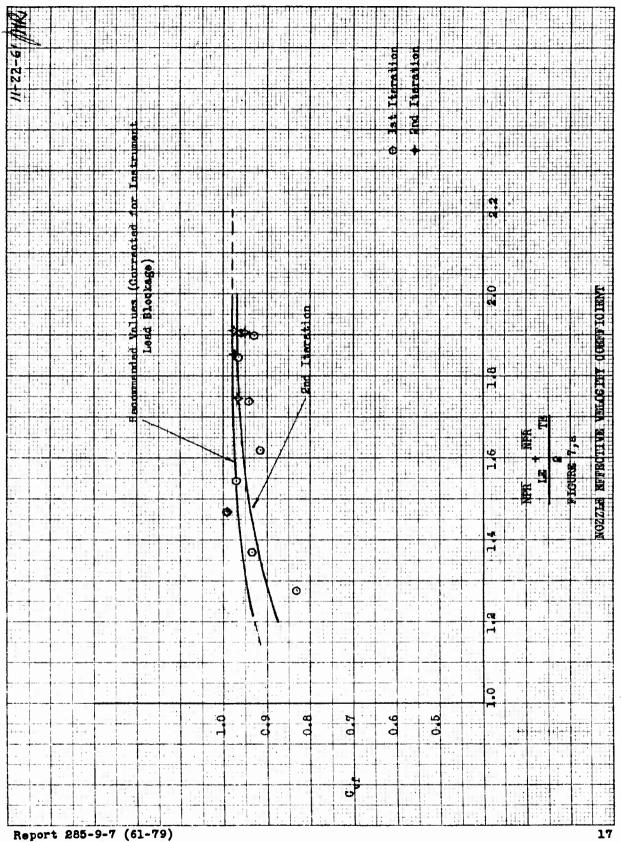
Substitution in equation (2) yields

$$(0.888 + 0.031) = (0.968 + \Delta C_{vf}) (0.919 + 2 \Delta C_{vf})$$

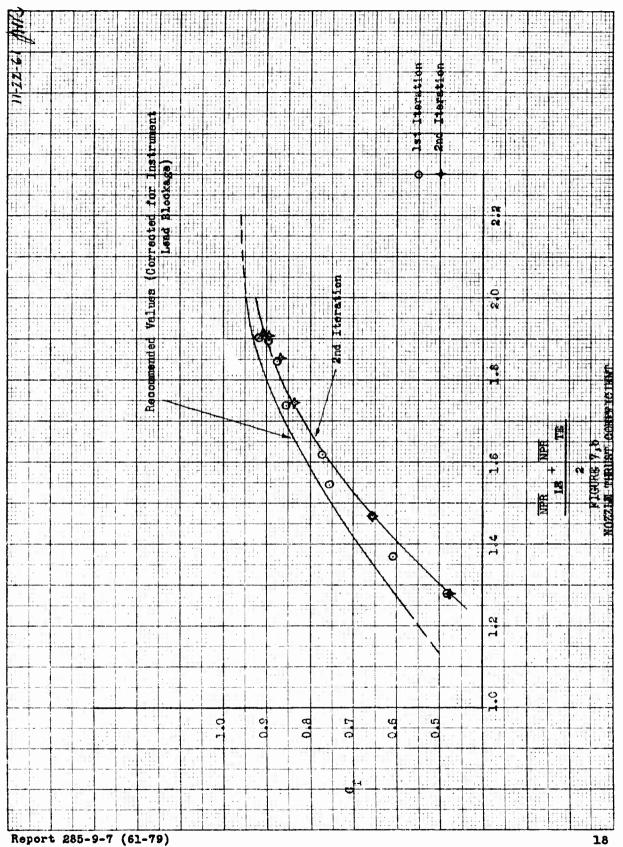
from which

$$\Delta C_{vf} = 0.01$$

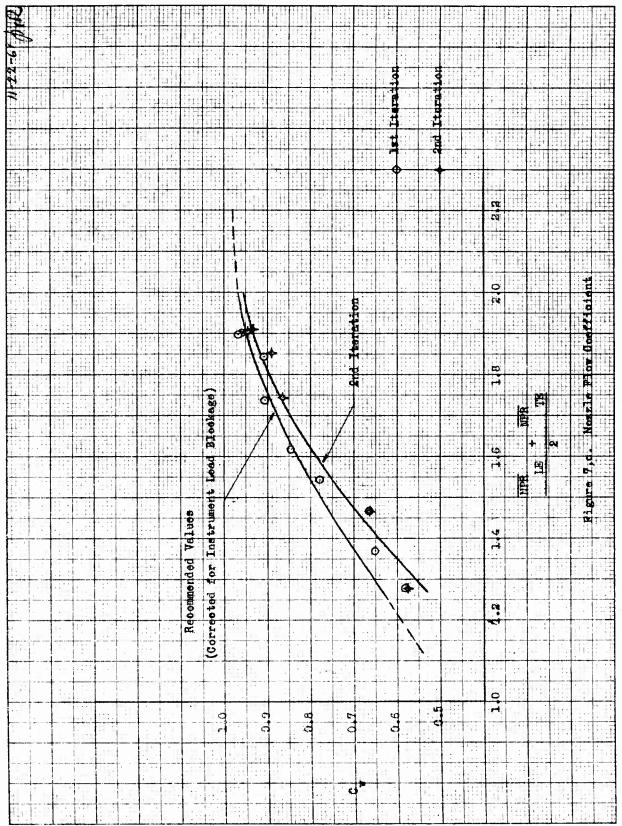
This correction was applied to the second iteration value (measured coefficients for blocked nozzle) of Figure 7 at NPR = 1.86 to provide the recommended nozzle coefficient.



17



18

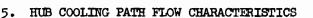


Report 285-9-7 (61-79)

4-RURALT 0->-0-0Z

From Figures 7a, b, and c, which correspond to a non-rotating blade, it is seen that the effect of nozzle pressure ratio on nozzle coefficients diminishes with increasing pressure ratio. In fact, at pressure ratios above 2, the coefficients are virtually unchanged. For a whirling blade and similar engine conditions, the major blade centrifugal pumping effect is a higher nozzle pressure ratio than those measured statically and therefore corresponds to nozzle coefficients at a level indicated by the dashed lines in Figure 7.

Two additional causes produce higher nozzle pressure ratios than those measured statically. First, the maximum engine pressure ratio of the T64 (engine for flight system) is 2.8 versus 2.5 for the whirl test J57 engine; and second, the whirling aerodynamically loaded rotor produces a tip vortex which lowers the local external back pressure causing a higher nozzle pressure ratio than if the whirling blade were unloaded (i.e. no tip vortex due to lift). All of these effects produce higher nozzle pressure ratios in a region where the effect of pressure ratio on nozzle coefficients is small.



The hub area is cooled by induced air flow due to centrifugal pumping (Figure 8). To determine the adequacy of the ejection ports and to ascertain the pressure loss characteristics of this path as a function of flow rate, ducts were connected to the exhaust ports (Figure 9) and a blower was provided to suck air through the hub circuit. The pressure loss was measured from ambient to a station several diameters forward of flow measuring orifices (Figure 10). With the ducts disconnected from the blade while maintaining the same flexible duct shapes, the pressure loss from ambient to the same station forward of the orifice was measured. The difference between the two pressure drops corrected by deviations from the flight flow circuit then provided the pressure loss of the hub path as a function of flow rate. This pressure loss when balanced with the centrifugal pressure rise establishes the hub circuit flow rate as a function of rotor rpm or tip speed.

Extrapolation of the flow data for rates in excess of 0.4 lb/sec was necessary due to blower limitations. For flow rates below this value, the data provided $\Delta P_{\rm t}/q$ vs w values which were sufficiently constant to allow extrapolation.

For incompressible flow, the rate of change of momentum of a mass segment due to centrifugal forces is (Reference 2),

$$\rho \, v \, d \, v = \frac{V_T^2 \, \rho \, r \, d \, r}{1 \beta} \, , \qquad (1)$$

Over the radial length $(r_2 - r_1)$ of the circuit, Equation (1) integrates to

$$q_2 - q_1 = \frac{\rho V_T^2}{2 g L^2} (r_2^2 - r_1^2),$$
 (2)

With an atmospheric intake and exhaust

$$P_{amb} = P_{t_1} = P_1 + q_1
P_{t_2} = P_{amb} + q_2.$$
(3)

Thus, from Equations (3),

$$\Delta P_{t_{QP}} = P_{t_2} - P_{t_1} = P_{amb} + q_2 - P_1 - q_1 = q_2 , \qquad (4)$$

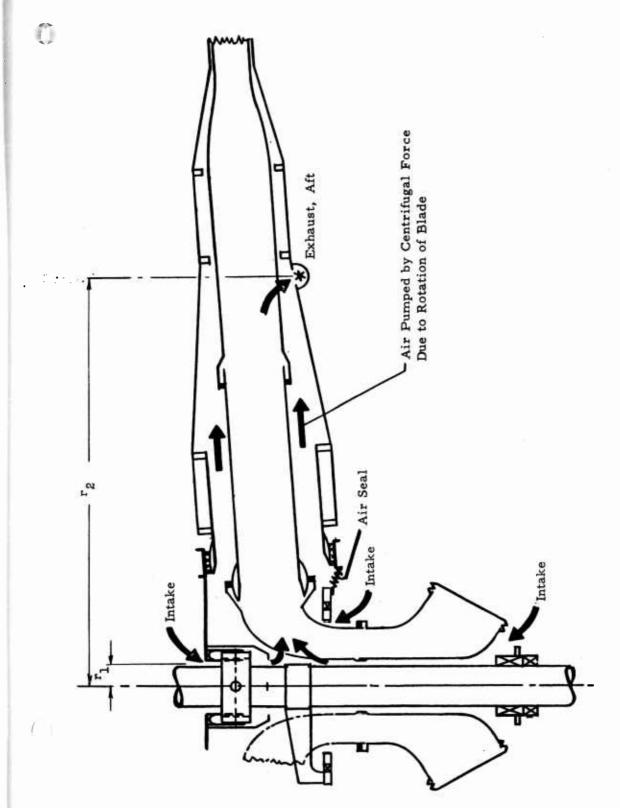


Figure 8. Schematic of Cooling System for Hub and Blade Root Components

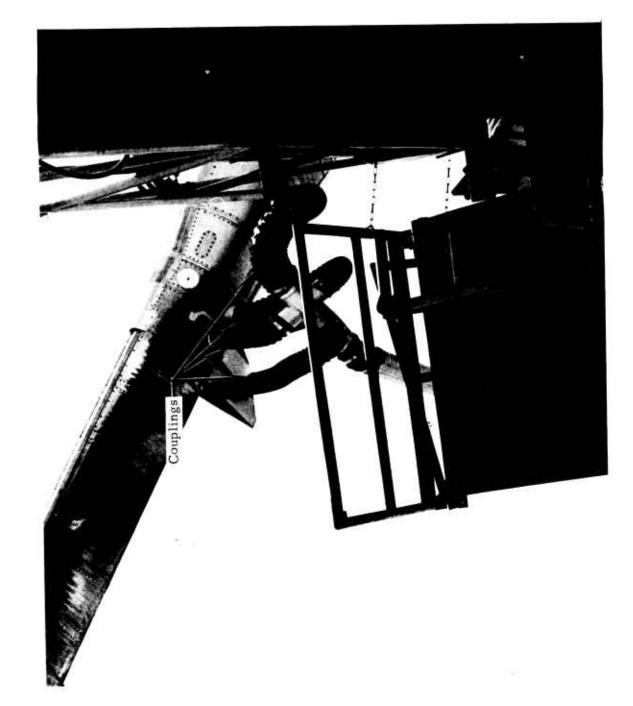


Figure 9. Typical Flexible Couplings Attached to Blades for Tether Operation and Hub Cooling Calibration

22



Report 285-9-7 (61-79)

and combining Equations (2) and (4)

$$\Delta P_{t_{of}} = q_1 + \frac{\rho V_T^2}{2 g L^2} (r_2^2 - r_1^2). \qquad (5)$$

Now, since the hub circuit inflow is near the rotor axis, $r_1 \approx 0$ and due to the large inlet area $q_1 \approx 0$. For the hub then, Equation (5) simplifies to

$$^{\Delta P_{t_{of}}} \approx \frac{^{\rho V_{T}^{2} r_{2}^{2}}}{2 g L^{2}} = \frac{^{r_{2}^{2} V_{T}^{2} \delta}}{288 g L^{2} R \Theta} \times \frac{14.7}{519}. \tag{6}$$

The air is exhausted through five ports of varying area at different radii from the hub centerline. The mass flow through a number of exhaust holes can be represented by

$$\mathbf{w}_{\text{tot}} = \sum_{\mathbf{n}} \mathbf{w}_{\mathbf{n}} = \sum_{\mathbf{n}} \mathbf{c}_{\mathbf{d}_{\mathbf{n}}} \mathbf{A}_{\mathbf{n}} \sqrt{\frac{P_{\mathbf{n}} \mathbf{v}_{\mathbf{T}}^{2} \mathbf{r}_{\mathbf{n}}^{2}}{2 \mathbf{g} \mathbf{L}^{2}}}.$$
 (7)

Assuming the discharge coefficient C_d to be equal for each exhaust port and assuming incompressible flow, Equation (7) may be written as

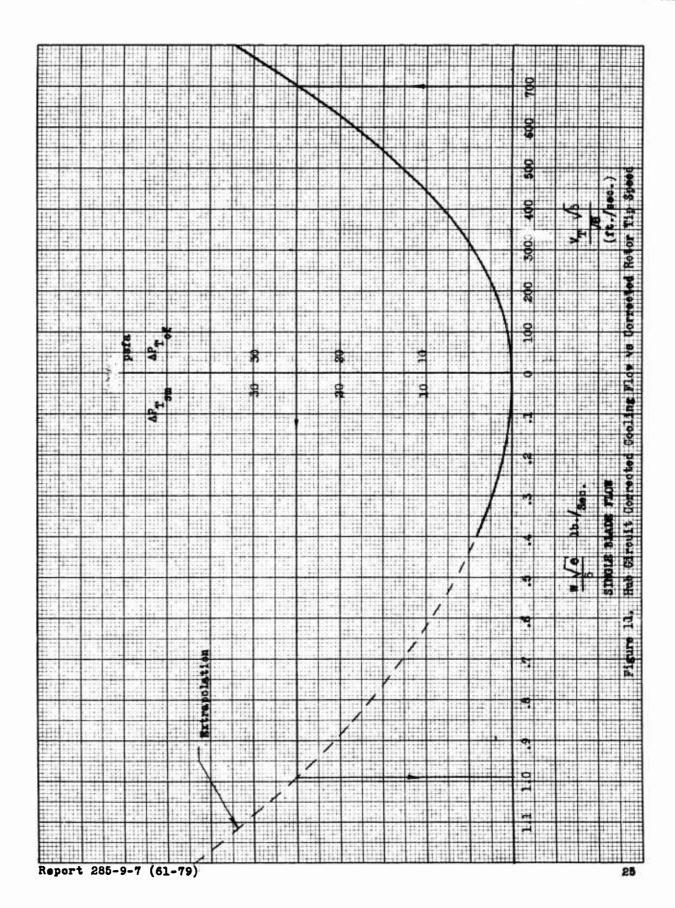
$$w_{\text{tot}} = c_{d} A_{\text{tot}} \sqrt{\frac{\rho V_{T}^{2} r_{\text{eff}}^{2}}{2 g L^{2}}} = n^{\sum C_{d}} \sqrt{\frac{\rho_{n} V_{T}^{2} r_{n}^{2}}{2 g L^{2}}},$$

from which an effective radius based on total discharge area may be defined as

$$r_{eff} = \frac{\sum_{n=1}^{\infty} A_n r_n}{A_{tot}}.$$
 (9)

Substituting this value of $r_{\rm eff}$ for r_2 in Equation (6) and utilizing the test data previously described results in the nomographic plot of Δ $P_{\rm cf}$ vs $\frac{V_{\rm T}}{\delta}$ and Δ $P_{\rm t_{sm}}$ (statically measured) vs $\frac{\sqrt{\Theta}}{\delta}$ as presented in Figure 11. From this figure, the hub cooling flow rate as a function of altitude ambient conditions and rotor tip velocity is quickly ascertained. For sea-level standard-day conditions, it is seen that the required flow rate of approximately 1 lb/sec per blade as assumed in previous thermal analyses is achieved.

Report 285-9-7 (61-79)





6. GAS GENERATOR INSTALLATION AND OPERATING CHARACTERISTICS

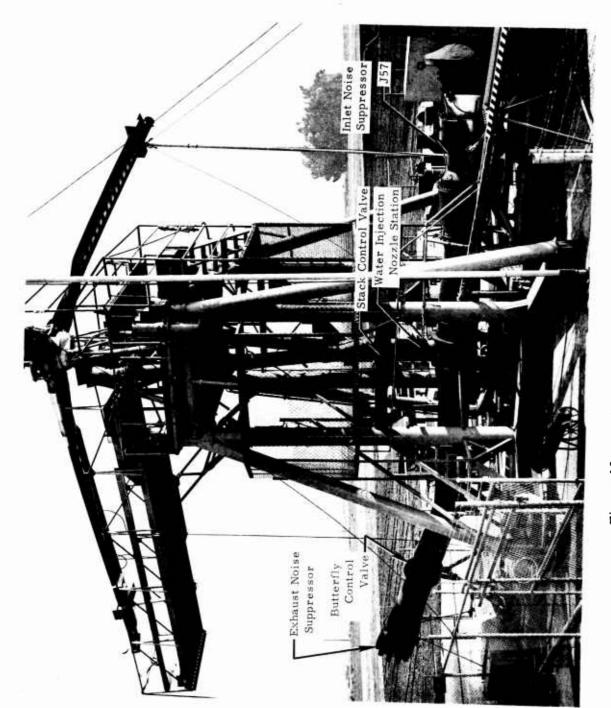
The J57-P-19W turbojet engine was selected as the whirl test gas generator since it is the most reliable engine currently available that suitably approximates the turbine discharge conditions of the T64 engine proposed for the Hot Cycle Helicopter. The large differences in air flow between these engines is accommodated by dumping approximately 60% of the J57 exhaust gas through a butterfly valve which also serves as a means of varying the engine operating line to achieve planned test conditions.

6.1 Installation

The J57 is installed at the base of the whirl test stand as shown in Figure 12. The reversibility of the engine mounting structure facilitated the initial power plant operation for familiarization and gas generator calibration with the standard turbojet nozzle. Approximately one-third of the hot gas from the J57 is removed from the main exhaust duct and directed into the rotor blades through a vertical duct system in which the gas temperature and pressure distribution is accurately measured. The unused engine exhaust is ducted aft where a butterfly dump valve controls the pressure within the system.

Normal installation practices are adhered to as detailed in Reference 3. While the whirl test engine installation is considered to be such that sufficient external engine cooling could be obtained for normal engine operation, temperature sensors of prototype installation type (Reference 3) are utilized due to projected operation above the normal engine operating line.

During the planned series of tests, considerable operation is to be conducted at very low engine power settings, especially during the initial whirl tests. The engine fuel flow which normally acts as the means of removing heat from the engine oil is not great enough to avoid over-temperature of the oil during prolonged



Report 285-9-7 (61-79)

operation of this type. For this reason, a pair of hydraulically driven engine oil-to-air coolers is utilized (Figure 12).

Engine throttle control is maintained from the mobile control van by a hydraulic servomechanism located on the blade collective pitch stick. Emergency throttle cut-off is available instantly through the use of a hydraulic accumulator which discharges high pressure fluid into the throttle servo when electrically actuated.

6.2 Initial Operation and Calibration

The first engine operation was conducted on May 17, 1961 in the presence of Pratt and Whitney Service Corporation personnel. Operator familiarization was completed at that time.

The engine calibration was conducted to determine the normal engine operating line with the standard jet nozzle. This was done to avoid deviations from normal engine operation during transients when the J57 gas generator is connected to the Hot Cycle test system. Figure 13 shows the engine installed in the calibration position with the direction of flow reversed 1800 from the normal whirl test position.

Complete engine operation data were obtained and all external temperatures were monitored. The results of the engine calibration are shown in Figures 14 through 16 where turbine discharge total temperature, total pressure, and fuel flow are shown as functions of high pressure compressor rpm. The humidity correction for fuel flow is presented in Figure 17. Figure 18 which indicates the variation of turbine discharge pressure with temperature for both the J57 and T64, provides a comparison of the relative performance capabilities of the test and flight gas generators.

Since the high power operation of the J57 is limited by engine pressure and rpm, the maximum temperature, Tt7, obtained during on-line operation was 1036°F.

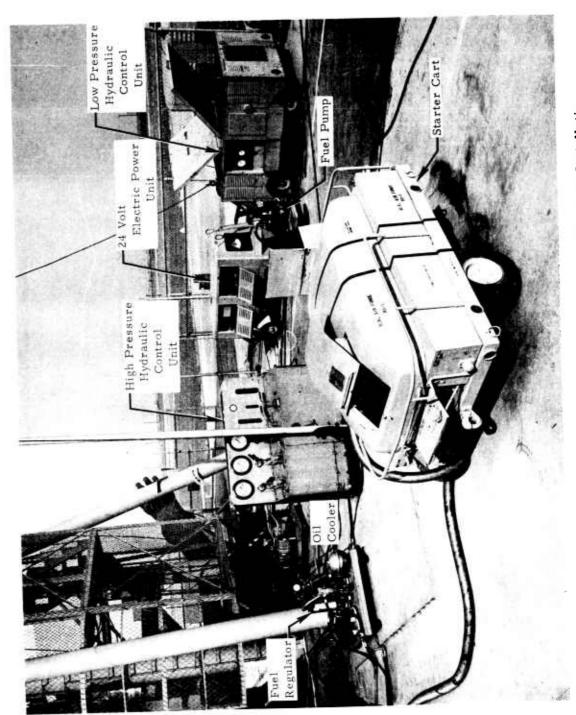
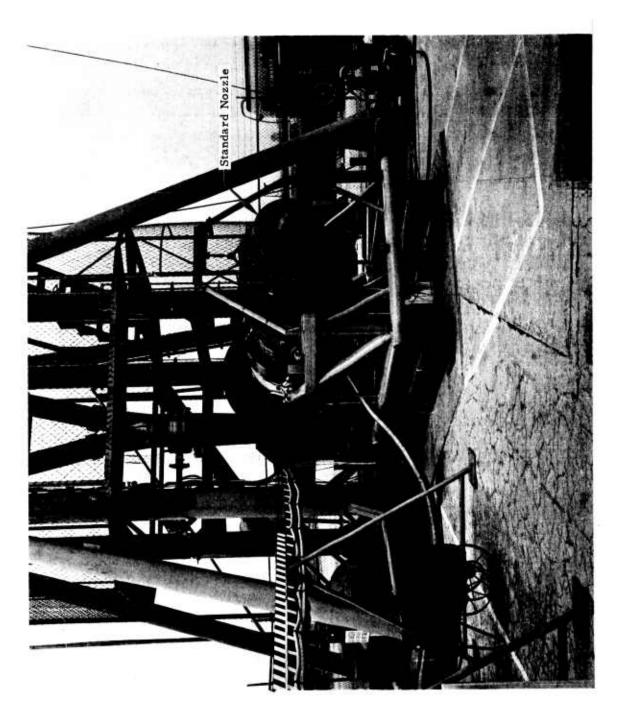
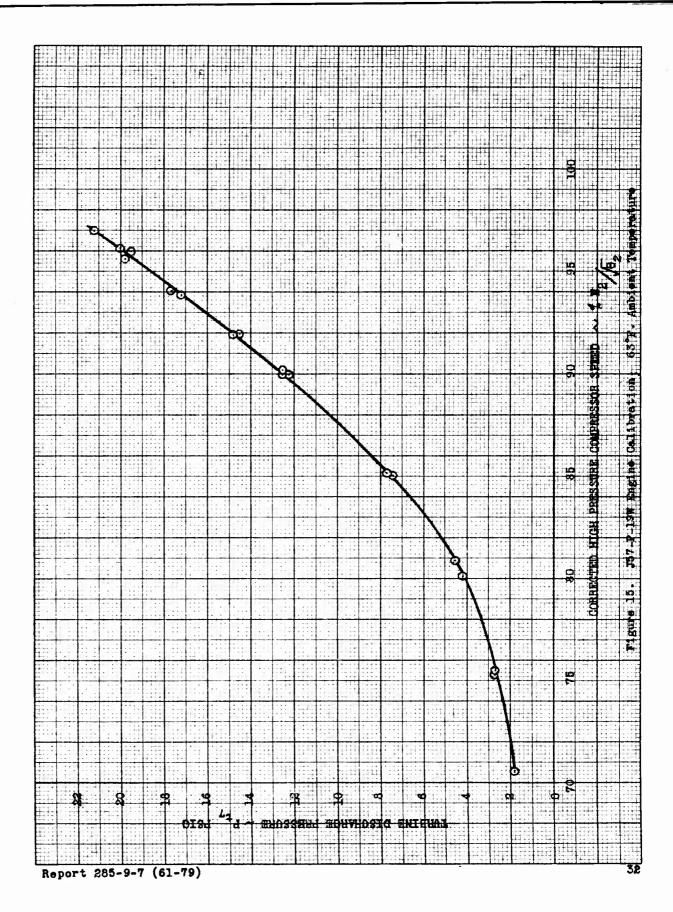


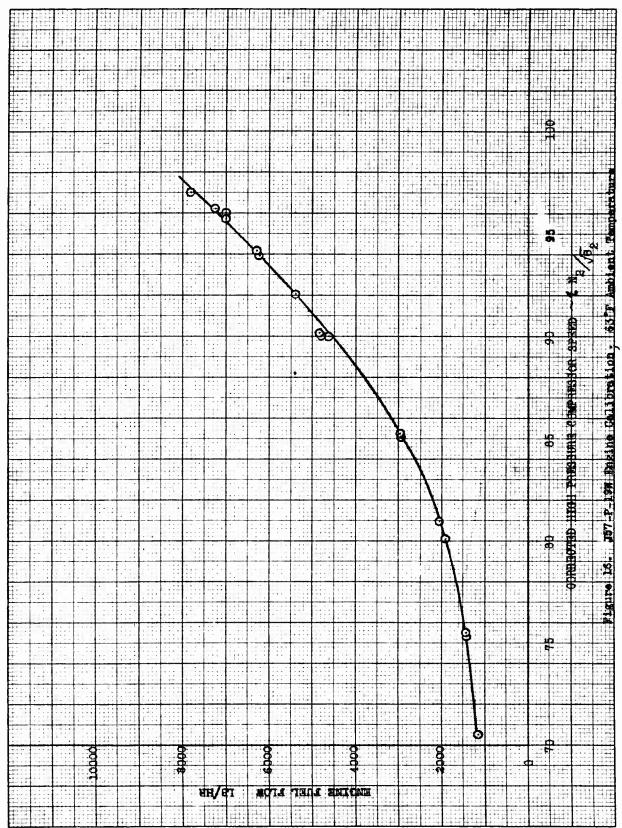
Figure 12, b. Auxiliary Power and Cooling Units for Whirl Test Installation



30

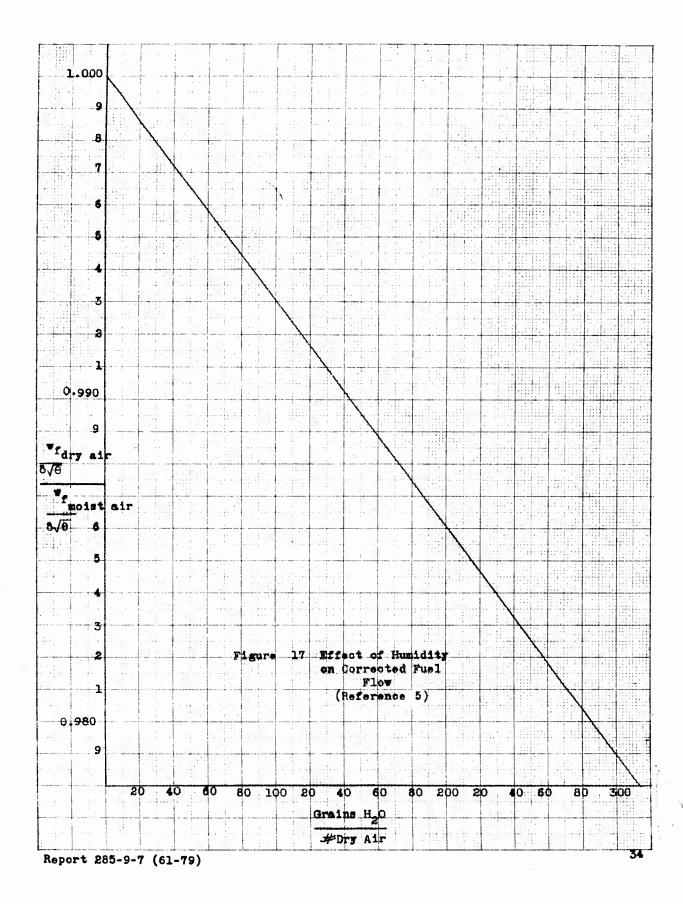
359-11 TO X TO TO THE % INCH



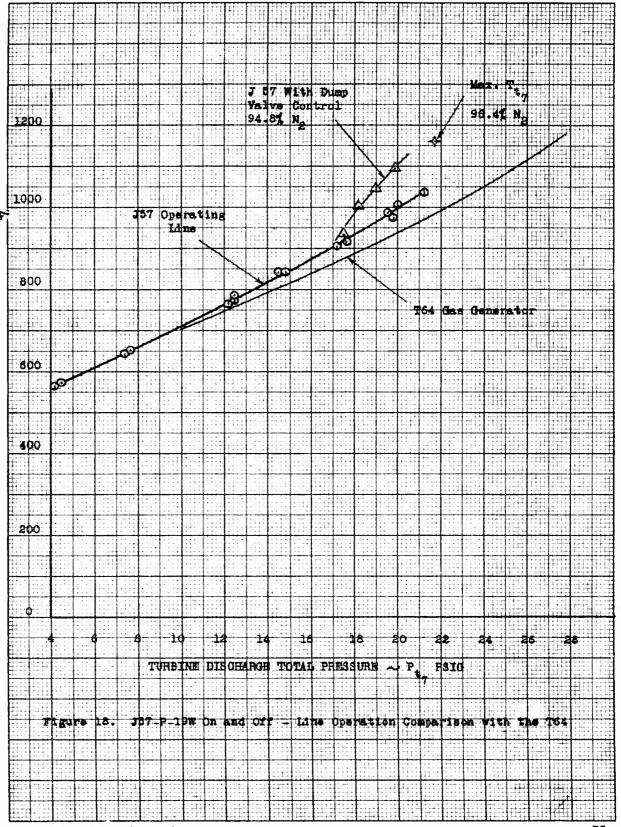


Report 285-9-7 (61-79)

33



TURBINE DISCHARGE TOTAL TEMPERATURE ~



Report 285-9-7 (61-79)

As stated earlier, however, the dump valve does provide for controlled off-line operation to achieve the required temperatures at less than maximum rpm without exceeding the engine pressure ratio limits of Reference 4.

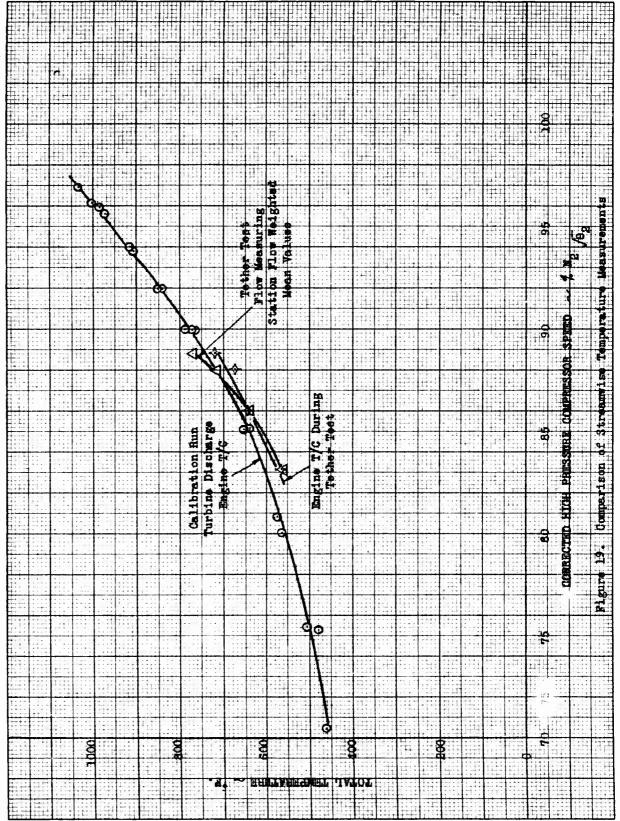
Following the engine calibration, the J57 was installed with the jet nozzle removed and the turbine casing mated directly to the whirl test duct as shown in Figure 12. With the upper butterfly valve closed to avoid flow through the then installed rotor blades, a series of engine runs were made to determine the off-line exhaust gas temperature capabilities and the sensitivity of the engine to sudden transients initiated by rapid dump valve movement.

The variation of T_{t_7} with P_{t_7} is shown in Figure 18 for off-line operation at constation No. This operation was conducted above the normal operating line thereby resulting in lower than normal low pressure compressor speeds indicating a decrease in airflow due to the smaller flow area at the choked valve. Again, noting Figure 18, it is seen that the maximum turbine discharge temperature attained was 1160°F at maximum engine pressure ratio. It should be noted that this turbine discharge temperature is not considered to be the maximum obtainable. since operation closer to the compressor stall line would yield a higher temperature but would possibly result in non-destructive compressor instability.

6.3 System Tests

There have been no engine difficulties encountered which have caused delays. However, a discrepancy was found between the exhaust gas temperature as measured at the turbine discharge by the engine furnished thermocouple assembly and the temperatures indicated by the flow measuring station instrumentation. This deviation is shown in Figure 19 for a limited range of temperature.

i



Report 285-9-7 (61-79)

7. SUMMARY

This report covers the analyses and experimental findings of static tests of internal flow channels of the Hot Cycle system. Pertinent results are as follows:

- a. Maximum thrust recorded was 702 lb/blade (9.6% water injection, $T_{t} \approx 730^{\circ}F$) which was consistent with the prevailing nozzle pressure ratio and gas temperature.
- b. Test derived values of the tip nozzle coefficients substantiate those which were predicted and used in past performance analyses. The previously assumed effective velocity coefficient of 0.955 and flow coefficient of 0.96 were repeatedly achieved or exceeded in the near choked and choked nozzle flow ranges. At nozzle pressure ratios above 1.75 the effective velocity coefficient (C_{vf}) was found to be 0.98, and the flow coefficient (C_{w}) was found to be increasing from 0.935 at NPR = 1.86 to 0.98 at NPR = 2.2. Figure 7 shows the recommended values of all coefficients.
- c. Primary duct pressure loss characteristics are essentially in agreement with predictions. This report covers the test period up through the tether test. Through that time, only that test provided adequately high flow rates to estimate duct losses. Unfortunately, this test provided a 3:1 unbalance of flow in the two parallel stacks. This notwithstanding, agreement between analyses and tests was observed for the stack ducts. The use of a single blade for thrust measurement yielded large pressure losses in the hub by causing flow mal-distributions (amplified secondary flow). The estimated turning losses in the hub were of the order of 4% Pt, which is approximately 300% greater than the full scale model tested value (3 blades) of Reference 6 which is more realistic.

- The pressure loss and centrifugal pumping characteristics of the hub cooling circuit were ascertained. Statically tested pressure losses when compared with calculated centrifugal pressure pumping capability of the hub circuit indicate that the provided blade cooling air ejection ports are adequate. For whirl tests at 800°F and 50% design rpm, there has been no problem with hub or spar cooling. A detailed temperature survey of the blade and hub is contained in Reference 9.
- e. No problems with engine function have evolved. Turbine discharge temperature in excess of 1160°F and engine pressure ratios of 2.48 have been achieved.
- f. The flow data analysis procedures have been established. Installed test instrumentation has proven satisfactory to allow correlation of analysis and test. Particularly, redundant data have yielded encouragingly similar results.

8. REFERENCES

- 1. Knudsen, J. G. and Katz, D. L.; "Fluid Dynamics and Heat Transfer";
 McGraw-Hill Book Co., Inc., 1958.
- 2. Henry, J. R.; "One-Dimensional, Compressible, Viscous Flow Relations Applicable to Flow in a Ducted Helicopter Blade"; NACA Technical Note 3089, December, 1953.
- 3. Pratt and Whitney Aircraft; "Gas Turbine Installation Handbook, JT3
 Turbojet Engines; Vol. 1"; May, 1956
- 4. Pratt and Whitney Aircraft; "Specific Operation Instructions J57-P-19W; Turbojet Engines"; Operation Instruction 138; July 1, 1957.
- 5. Sameuls, J. C. and Gale, B. M.; "Effect of Humidity on Performance of Turbojet Engines; NACA Technical Note 2119, June, 1950.
- 6. Boswell, C. C. and Thurston, S.; "Results of Component Test Program; Hot Cycle Rotor System"; Hughes Tool Company - Aircraft Division Report 285-9-4; August 30, 1957.
- 7. Keenan, J. H. and Kaye, J.; "Gas Tables"; John Wiley and Sons, Inc.; 1948.
- 8. Lancaster, O. E.; "Jet Propulsion Engines": Princeton University Press, 1959.
- 9. Amer, K. B.; "Whirl Tests, Item 7a"; HTC-AD Report 285-16 (62-16); March 1962.

9. NOMENCLATURE

9.1	Symbols	3

- A Area
- Od Discharge coefficient; ratio of actual to ideal discharge; term generally associated with incompressible flow; equals the flow coefficient
- $C_{\mathbf{f}}$ Thrust coefficient; ratio of actual to ideal thrust
- C_{vf} Effective velocity coefficient; ratio of effective velocity assuming complete isentropic expansion to ideal fully expanded velocity
- C Flow coefficient; ratio of actual to ideal flow
- c Specific heat at constant pressure
- EPR Engine pressure ratio
- F Thrust
- g Acceleration due to gravity
- h Static enthalpy
- J Mechanical equivalent of heat
- L Rotor length; distance from & to nominal center of nozzle: 320 in.
- M Mach number
- N Low pressure compressor % speed
- N, High pressure compressor % speed
- NPR Nozzle pressure ratio based on mass weighted nozzle inlet total pressure
- P Pressure; no subscript for static values
- Q Lower heating value of JP-4 fuel; 18,400 Btu/lb
- q Dynamic head (incompressible)
- R Gas constant
- r Radius or radial station

- T Temperature; no subscript for static values
- $\mathbf{v}_{\mathbf{T}}$ Rotor Tip Velocity based on 320 in. radius
- Velocity
- Flow rate
- Pounds

Ratio of specific heats

- Δ Differentail
- δ Pressure parameter; equals P/14.7
- Efficiency
- Temperature parameter; equals T/519
- Density

- 40
- 9.2 Superscripts
- Mass weighted values
- * Sonic conditions
- 9.3 Subscripts
- a Air
- act Actual or physical value
- amb Ambient
- avg Average
- B Burner
- of Pertains to centrifugal force
- d,e,f Station designations for Section 11
- edge Total pressure probe location near wall to pick up "near" boundary layer effects
- eff Effective
- oil Engine lubricating oil
- f Fuel
- fs Flow measuring station in parallel stacks
- g Gross or gas
- hub Hub station below rotating seal
- Report 285-9-7 (61-79)



- () is Isentropic
- LE Blade leading edge duct
- Maximum; values along duct centerline ma.x
- Summation digit
- Nozzle inlet plane nozz
- Statically measured value (blade tethered) sm
- TE Blade trailing edge duct
- Total or stagnation
- tot Total or sum
- Wall
- 0 Free stream
- General radial station designations in Section 5 1,2
- 2 Compressor inlet station
- 7 Turbine discharge station
- Branch I from Figure 1 I
- Branch II from Figure 1 II



10. APPENDIX I; FLOW DATA ANALYSIS

This section established the procedures for flow data analysis used in this report. Resulting engine and flow parameters for the tether test are given in Table 3. Note: The dimensions included in this table are those directly read from the instruments or are in engineering absolute quantities to aid quick calculations of other values not directly presented herein.

The use of Nikuradse's data (Reference 1) to determine flow rate affords a simplification and reduces the data analysis effort (See Section 10.2). However, while the velocity profiles are suitably developed at the nozzle inlet station (lead-in duct is straight and has a large length to diameter ratio), a check was made to determine the adequacy of this method at the flow measuring station.

From Figure 20, it is seen that the velocity profiles in Branch II are not quite symmetric and considerably flatter than those due to Nikuradse (See Figure 22). This is attributed to the assymetry of the flow duots, a relatively short straight lead in, and flow unbalance in the branches (See Section 2). Column 22 of Table 3 indicates that the use of Nikuradse's data leads to a +6 to 7% error. It is concluded, however, that a further check is warranted when the blades are untethered and design flow rates are being measured.

10.1 Flow Measurement

The procedure for determining flow at the twin stack measuring stations (Figure 21) and the nozzle inlets is to assume a turbulent velocity profile similar to those of Nikuradse's. Thus, based on the total pressure at the center of the duct corresponding to maximum velocity and static pressure measurements at the wall, the average velocity can be ascertained once having integrated Nikuradse's profiles to determine the ratio of average to maximum velocity as a function of Reynolds number.

Report 285-9-7 (61-79)

10 X 10 TOTHE CM. 359.14 KEUFFEL & ESSER CO. WATEHUSS A

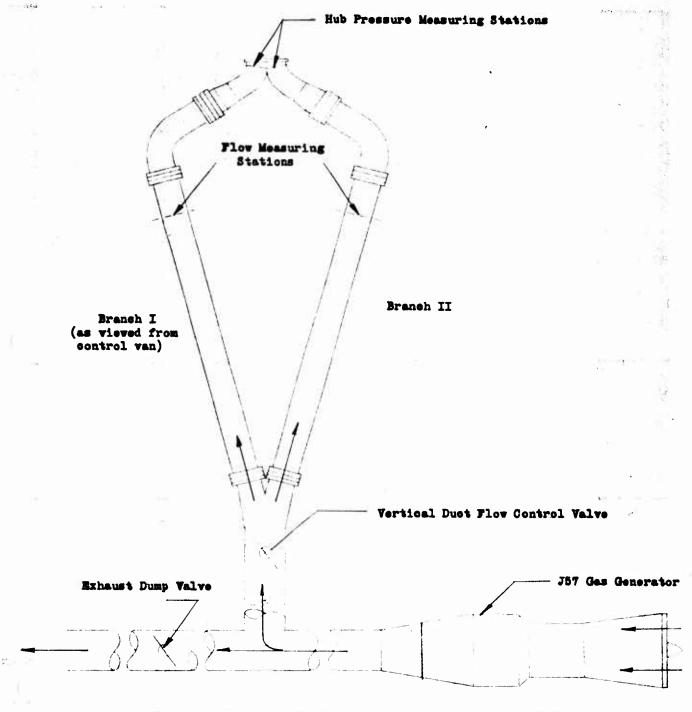


Figure 21. Permanent Streamwise Flow and Pressure Measuring Stations
Report 285-9-7 (61-79)

ALL AND LEVER KANDERS OF THE SECOND OF THE PROPERTY OF THE PRO



									HU	GHE	B TO:	OL CO	OMPANY	
							TAI	BLE 3						A-RORAET
					J57			FLOW P	Arameti Est	ers				
Run No •	1	2	3	1+	5	6	7	8	9	10	11	12	1.3	D->-0-0Z
NO.	Pamb	$\mathbf{T}_{\mathbf{amb}}$	Rel. Hum.	N_1	N ₂	$\mathbf{w_f}$	$^{\mathrm{P_t}}$ 7	Tt7	Poil	T_{oil}	EPR	$P_{ ext{thub}_{ extbf{I}}}$	$P_{ ext{thub}}$ II	20
	psfa	$\circ_{\mathbf{F}}$	%	%	%	#/sec	psfa	$\circ_{\mathbb{R}}$	psig	°C		psfa	ps fa	
1234567890112345678901234567	2117 2118 2118 2118 2118 2118 2118 2118	72 74 75 75 75 76 76 73 73 73 73 73 73 73 73 73 73 73 73 73	71 71 71 71 71 71 71 71 71 71 71 71 71 7	70.0 711.0 80.0 81.2 100 83.2 95.2 95.2 95.2 95.3 87.8 87.8 87.8 97.2 97.2 97.3 97.3 97.3 97.3 97.3 97.3 97.3 97.3	86.5.2.5.5.9.0.8.0.5.5.8.8.8.3.3.8.0.0.8.8.2.3.3.8.9.9.9.9.9.9.9.9.9.9.9.9.9.9.9.9.9	0.750 0.833 1.111 1.278 1.333 1.528 1.944 1.750 1.722 1.889 1.667 1.667 1.667 1.6611 1.611 1.611 1.611 1.611 1.931 1.931 1.931 1.931 1.931	319774 3197774 3190624 49554 49588 49580 4	1148 1242 1310 1410 1495 1485 1580 1580 1550 1560 1560 1485 1495 1415 1425 1425 1426 1560 1560 1560 1560	47777788888888888887788888888888877888888	4555555554544455555555544455	1.510 1.632 1.782 1.884 1.986 2.149 2.339 2.353 2.099 2.353 2.097 2.361 2.151 2.070 2.070 1.897 2.353 2.354 2.354 2.355 2.354 2.355	3020 3291 3573 3806 3986 4309 4587 4735 4727 4727 4727	2972 3230 3505 3729 3908 4227 4499 4623 4630 4633 4624 4634 4618 4618 4613 4649 3449	

TABLE 3 (Contd.)

								н	JGHE	в то	OL C	OMP	any «	
-														A-RORAFT
						TABLE	3 (C	ontd.)						
			J	57 ENG	INE AND	FLOW	PARAM	ETERS	FOR TE	THER TE	ST			D->-@-0z
Run	14	15	Niku 16	radse M 17	iethod 18	Area 19	Integr 20	ration 21	22	Leadin 23	g Edge 24	25	26	8-0
No.	$\mathtt{T_{t_{I_{fs}}}}$	T _{tII} fs	wI	wII	wtot	wI	w _{II}	Wtot	1	P _t	Pt	Tt	NPR	7
	$\circ_{\mathbb{R}}$	o _R	#/sec	#/sec	#/sec	#/sec	#/sec	#/sec	%	psfa.	psfa	$\circ_{\mathbb{R}}$		
1 2 3 4 5 6 7 8 9 10 11 2 13 4 5 6 7 8 9 10 11 2 13 4 5 6 19 2 12 2 2 2 2 2 2 2 2 2 2 2 2 2 2 2 2	1025 1115 1182 1226 1055 1061 1030 1127 1129	1064 1160 1222 1275 1075 1078 1074 1080 1180	1.21 1.28 2.59 2.59 2.36 3.30 3.07 3.96 3.14 3.13	6.21 6.96 7.65 8.31 9.54 10.15 10.52 10.81	7.42 8.24 10.24 10.67 12.84 13.22 14.48 13.89 14.16	1.45 1.54 3.07 2.80 3.88 3.61 3.74 3.68 3.69	9.90 10.62 11.86	15.60 14.93	6.5 6.2 7.3 6.6 6.8 7.1 7.2 7.0	2716 2909 3109 3290 3449 3725 3949 4078 4086 3745 3306	2676 2861 3076 3218 3372 3646 3874 3980 3989	1018 1090 1180 1230 1060 1060 1068 1072 1150 1130	1.264 1.351 1.452 1.519 1.592 1.721 1.829 1.879 1.883	
	1188 1228	1228 1278								3813 3827 3834 3459 3487 3523 3509 3537 3536 3229 3225		1150 1190 1235 1215 1180 1150 1135 1180 1225 1135 1170		
23 24 25 26 27	1185 1145 1060 1173	1220 1175 1078 1220												

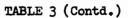
TABLE 3 (Contd.)

									HU	GHE	B TO(OL C	OMF	PANY	
									,						4-RORAET
						TABL	E 3 (C	ontd.)							
			J57	ENGIN	E AND	FLOW	PARAM	eters f	OR TET	HER TE	ST				D->-0-0Z
Run	27	28	ailing 1	94ge 30	3 1	32	33	34	35	36	37	38	39	140	
No.		Ptmax	F	Tt	NPR	٧	V _{tot} =27+28	Error 21-33 x1	.00 Wa 2	W _f /W _{e2}	% Theo Dry Air	H20	8	R	
	#/sec	psfa	psfa	o _R		#/sec	#/sec	21 %	#/200		*	*		frt/#OR	
1	4.06	2783	2736	1018	1.292	4.42	8.48	- 6.8	84.06	0.0089	760	0	1.373	53.35	
2	4.46	2997	2940	1095	1.388	4.83	9.29	- 5.3	80.46	0.0104	655	0	1.367	53.35	
3	3.93	3208	3144	1180	1.484	5.07	9.00	+18.6	97.74	0.0114	596	0	1.361	53-35	
h	5.38	3403	3224	1230	1.569	5.13	10.51	♦ 8.0	103.94	0.0123	551	0	1.356	53-35	
5	6,15	3563	3481	1070	1.644	6.32	12.47	- 9-5	103.30	0.0129	525	8.9	1.357	56.12	
6	6.52	3831	3740	1065	1.766	6.93	13.45	+ 5.5	107.22	0.0143	476	8.7	1.357	55-97	
7	6.55	4069	3971	1068	1.875	7.36	13.91	+10.8	138.00	0.0141	481	8.7	1.357	55-97	
8	7.49	4198	4093	1068	1.932	7.78	15.27	- 2.3	119.45	0.0147	463	9.0	1.357	56.05	
9	7.20	4206	4103	1150	1.937	7.43	14.63	+ 2.4	110.33	0.0156	14314	8.0	1.351	55.78	
10		3872		1128											
11		3441		1125											
12		3955		1150											
13		140014		1193											
14		4011		1240											
15		3622		1215											
16		3639		1180											
17		3678		1150											
18		3636		1140											
19		3657		1180											
20		3685		1225											
21		3352		1135											
22		3352		1170											

TABLE 3 (Contd.)

			1	Lead	ing Edge		Trail	ing Edge		ı		
Run	41	42	43	դդ	45	46	47	48	49	50	51	52
No.	C _{vf}	C _f	C _w	${ t P_t}$	NPR	w	$\overline{P}_{\mathbf{t}}$	NPR	w	Cvf	c _{f.}	C _w
1	0.831	0.482	0.580									
2	0.934	0.607	0.650			İ						
3	0.991	0.657	0.663									
4	0.972	0.756	0.778			l						
5	0.916	0.772	0.843									
6	0.941	0.853	0.906	3632	1.715	6.38	3722	1.757	6.76	0.968	0.837	0.865
7	0.966	0.876	0.907	3863	1.824	6.41	3950	1.865	7.19	0.974	0.868	0.891
8	0.929	0.897	0.966	3960	1.875	7.30	4067	1.920	7•59	0.950	0.897	0.944
9	0.959	0.918	0.957	3971	1.875	7.04	4085	1.929	7.28	0.974	0.910	0.934

First Iteration -> Second Iteration



Run No.	53 C _{vf}	Blockage Corrected 54	Values 55 C _W
1			
2			
3			
14			
5			
6	0.982	0.877	0.892

0.908

0.937

0.950

0.918

0.971

0.961

0.989

0.964

0.989

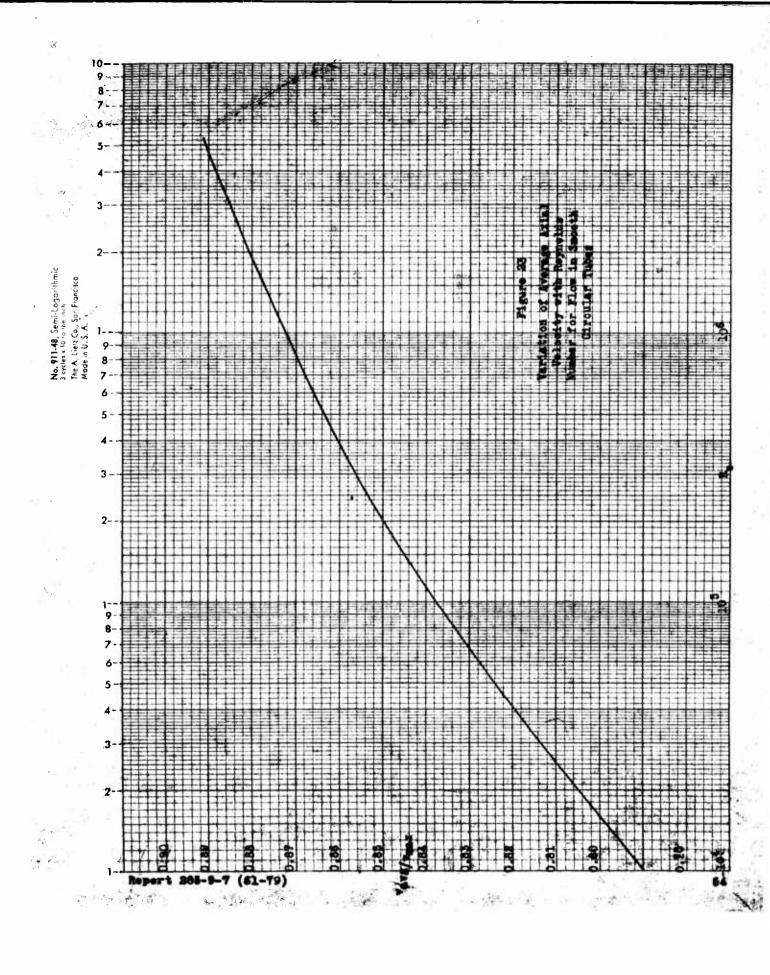
the stack measuring stations, as profiles against those of a finlet station must be based a circular and are thus Due to the short straight section leading into the stack measuring stations. additional total probes are provided to calibrate the profiles against those of Nikuradse. Also, an evaluation of flow at the nozzle inlet station must be based on hydraulic diameter since the blade ducts are non-circular and are thus different from Nikuradse's.

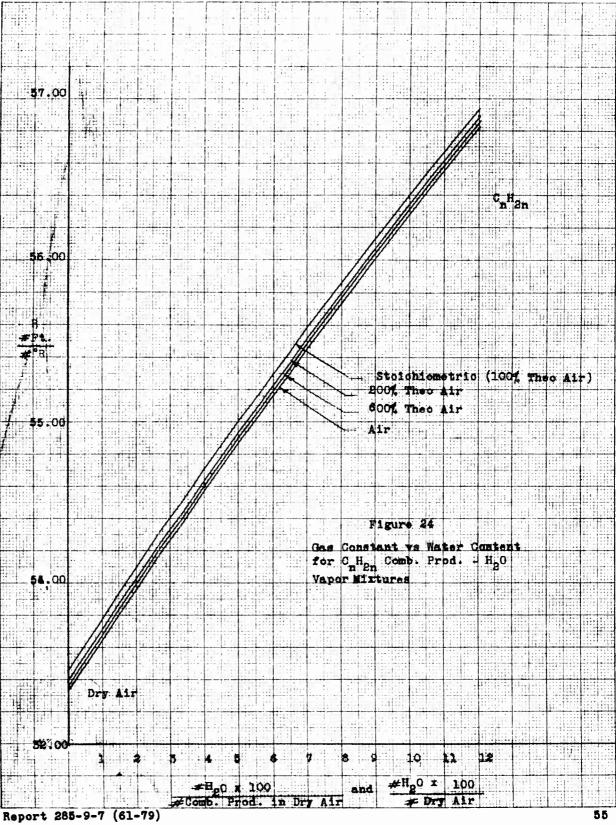
Nikuradse's velocity profiles for several values of Reynolds number are given in Figure 22. Included also on this figure are the radii at which pressure and temperature measurements are made at the stack measuring stations. Figure 23 presents the ratio of average to maximum velocity as a function of Reynolds number (Reference 1).

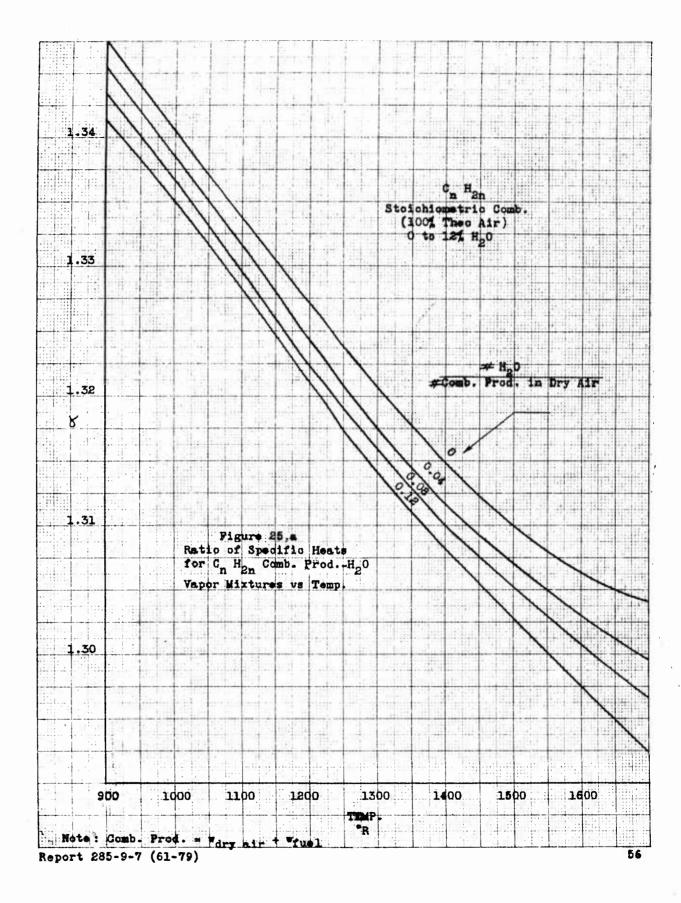
The analysis initially assumes the values of gas constant R and ratio of specific heats & to be 53.35 ft-lb/lbOR and 1.35 respectively. All analysis dependent values reported herein except those identified in Table 3 and the nozzle coefficient figures are 1st iteration values as it is felt that they are representative and additional iteration is not merited. The nozzle coefficients show about a 2 to 4% effect between iterations and therefore both values are provided for reference. The actual values are dependent on fuelair combustion ratio, temperature, and water content. The corrected R and X values are presented in Figures 24 and 25 and necessitate iterative analyses when they differ appreciably from the assumed values.

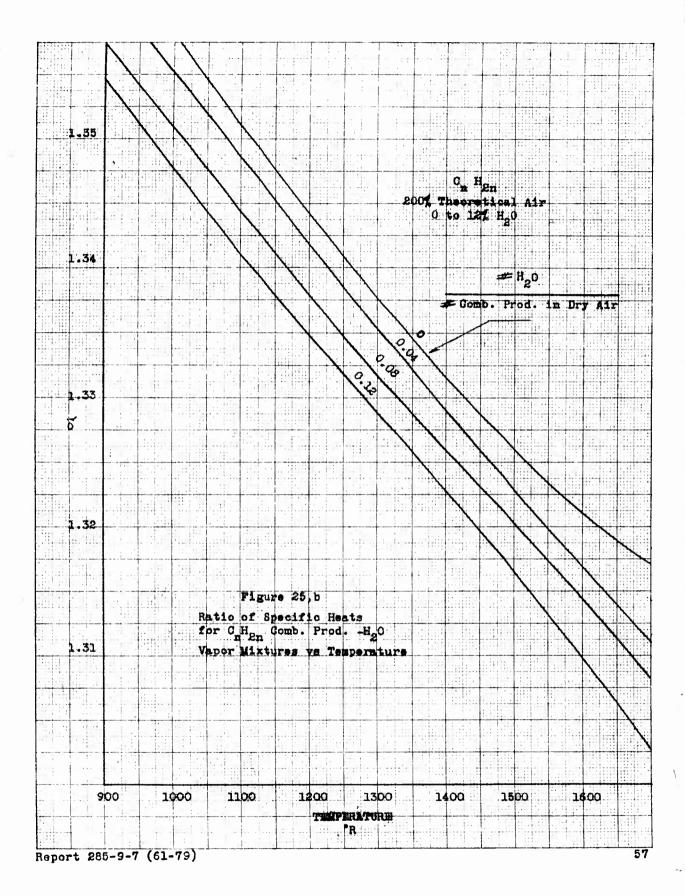
To determine the percentage of water in the primary stream caused by ambient humidity and cooling water injection, an enthalpy balance across the engine is made. This enthalpy balance establishes the engine air ingestion rate while ambient conditions and Figure 26 provide the water percentage due to humidity. The cooling water injection rates are measured directly to complete the input requirements (Figure 27).

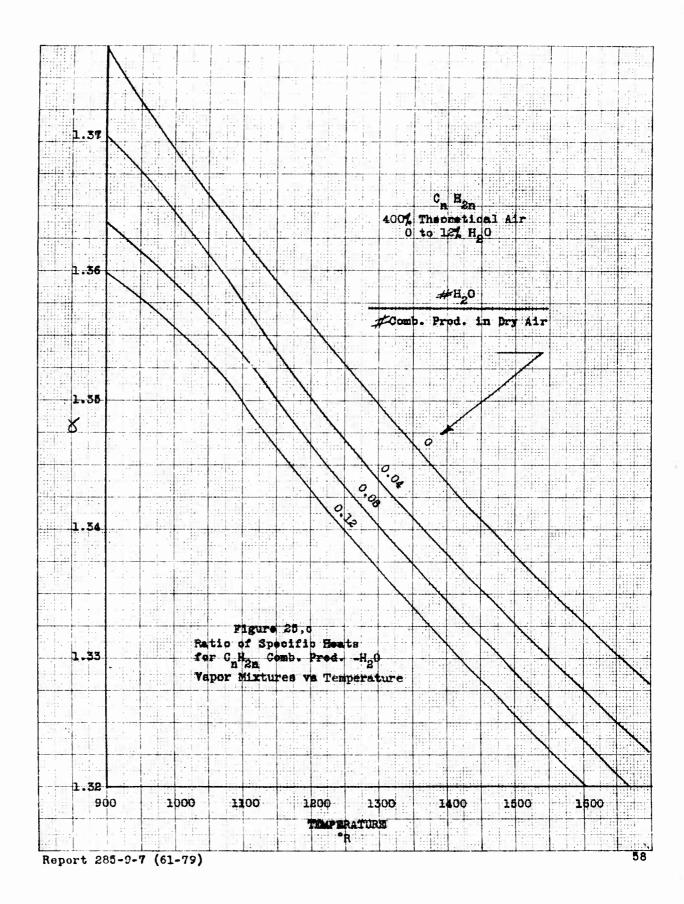
[SEDENT & SERENCE SESENCE SESENCE SERENCE SESENCE SE

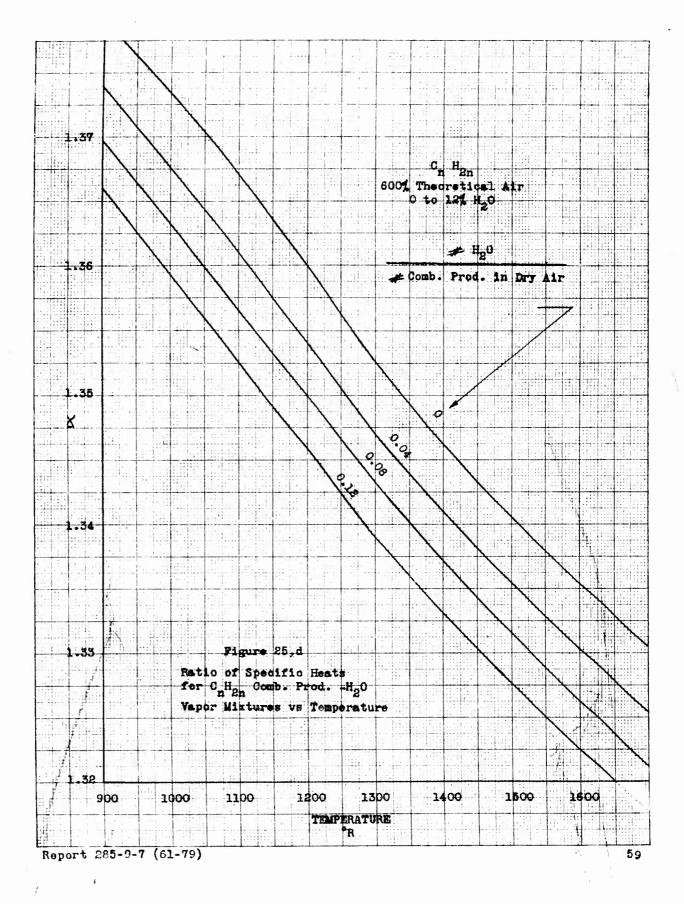


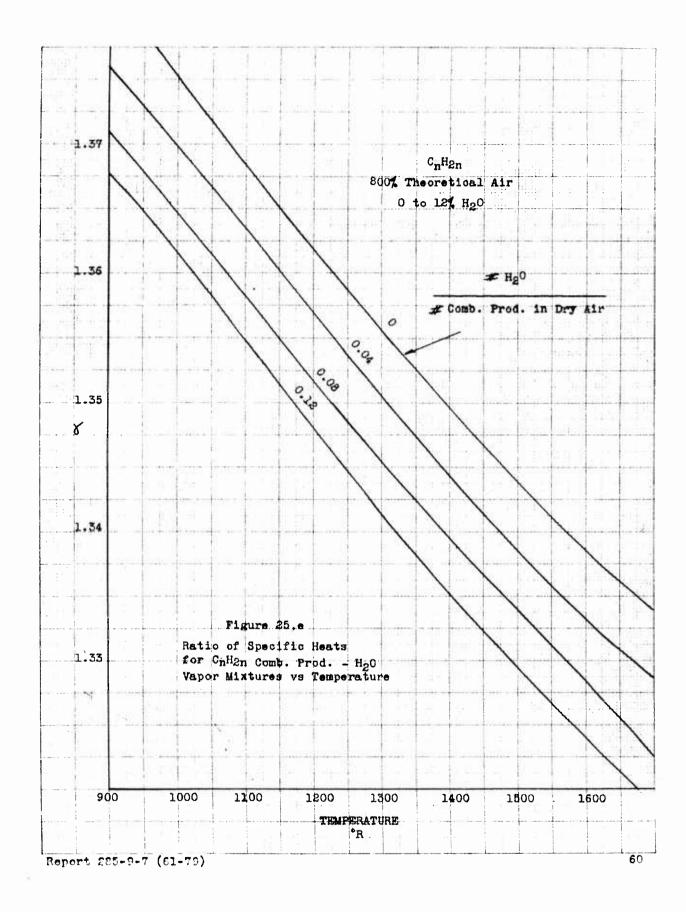


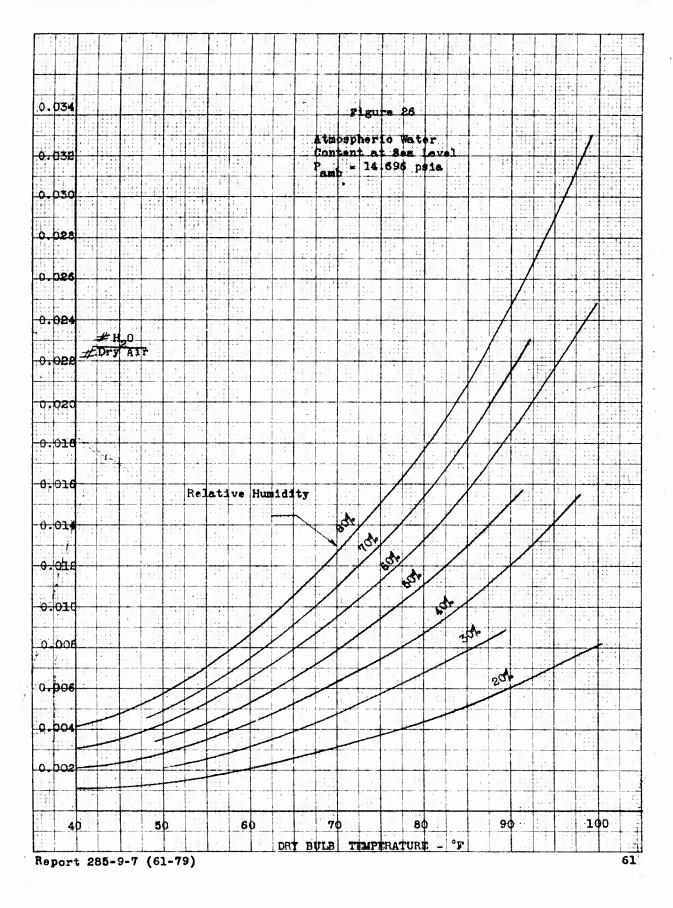


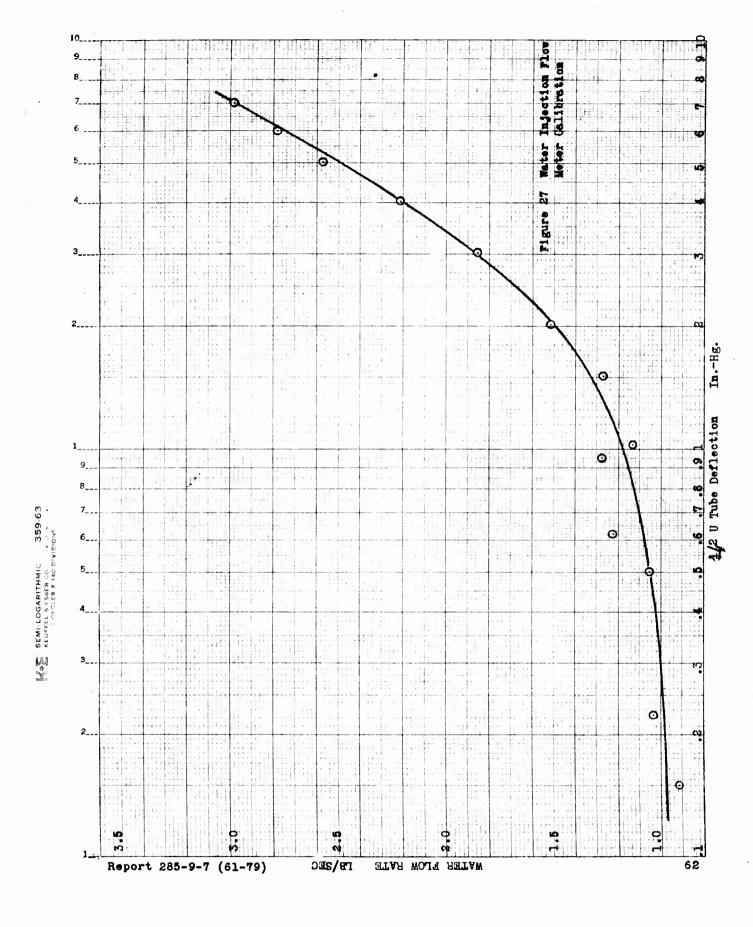












Ignoring compressor and turbine mechanical losses, a cycle enthalpy balance across the engine may be written as follows:

$$\mathbf{w}_{\mathbf{a}_{2}} \quad \mathbf{h}_{2} \quad + \quad \mathbf{\gamma}_{\mathbf{B}} \quad \mathbf{Q}_{\mathbf{f}} \quad \mathbf{w}_{\mathbf{f}} = \quad \mathbf{h}_{7} \quad \mathbf{w}_{7} \quad . \tag{1}$$

The engine air ingestion rate is then

$$\mathbf{w}_{a_{2}} = \frac{(\gamma_{B} Q_{f} - h_{7}) \mathbf{w}_{f}}{h_{7} - h_{2}}.$$
 (2)

The results for each run are presented in Table 3 for which the assumed values for calculation are

 $Q_p = 18,400 \text{ Btu/lb}$

 $\gamma_{\rm B} = 0.96$

 $h_0 = dry air values (Ref. 7)$

 $h_7 = 400\%$ theoretical air $(C_n H_{2n})$ values (Ref. 7)

10.2 Mass Weighted Nozzle Inlet Total Pressure

In order to establish a number of nozzle coefficients, a knowledge of nozzle inlet total pressure is required. For many cases, the velocity profile entering the nozzle is sufficiently flat to cause negligible error when using an average inlet total pressure based on several measurements in the nozzle inlet plane. For the rotor tip nozzles which are fed by ducts having a large length to diameter ratio, however, the nozzle inlet velocity profile provides quite a variation in cross section total pressure and necessitates an integration to determine the nozzle inlet mass weighted total pressure.

For M ≤ 0.5, the difference between total and static pressure may be approximated by

$$P_{t} - P \approx (1 + \frac{M^{2}}{4})q \tag{3}$$

or

$$P_{t} - P \approx \left[1 + \frac{1}{2(\sqrt[4]{t}-1)} \left(\frac{T_{t}}{T} - 1\right)\right] q.$$

Reducing the flow duots to their circular cylindrical equivalents, the mass weighted total pressure is defined by

$$\overline{P}_{t} = \frac{\int_{0}^{r_{w}} P_{t} dw}{P_{t} dw} = P + \frac{\int_{0}^{r_{w}} \left[1 + \frac{1}{2(\sqrt[4]{-1})} \left(\frac{T_{t}}{T} - 1\right)\right] \frac{\rho v^{2}}{2g} 2\pi r dr v \rho}{\int_{0}^{r_{w}} dw} (5)$$

which may be approximated by (X and R assumed constant across the duct),

$$\overline{P}_{t} \approx P \left\{ 1 + \frac{\frac{1}{2RT_{max}} \left[1 + \frac{1}{2(\sqrt{-1})} \left(\frac{T_{t}}{T_{max}} - 1 \right) \right] \int_{0}^{r_{w}} v^{3} r dr}{v r dr} \right\}$$
(6)

where T_{max} is based on M_{max} at the center of the duct. For the present study, this leads to an estimated \overline{P}_t which is less than 0.2% greater than the value received from an exact integration of Equation (5).

The universal velocity distribution for turbulent flow in smooth circular tubes is given by Reference 1 as

$$\frac{\mathbf{v}}{\mathbf{v}_{\text{max}}} = 1 - 0.204 \left(\frac{\mathbf{r}}{\mathbf{r}_{\text{W}}}\right)^2 - 0.250 \left(\frac{\mathbf{r}}{\mathbf{r}_{\text{W}}}\right)^{32} \tag{7}$$

Substitution of Equation (7) into (6) and integrating leads to

$$\overline{P}_{t} = P \left\{ 1 + 0.402 \left[1 + \frac{1}{2(\tilde{Y}-1)} \left(\frac{T_{t}}{T_{max}} - 1 \right) \right] \frac{v^{2}_{max}}{g R T_{max}} \right\}$$
and for $\tilde{Y}_{t} = 1.35$, $R = 53.35 \# ft/\#^{\circ}R$, and $\rho_{max} = \frac{P}{R T_{max}}$

$$\overline{P}_{t} = P + 0.803 \left[1 + 1.428 \left(\frac{T_{t}}{T_{max}} - 1 \right) \right] q_{max}.$$
 (9)

11. APPENDIX II; DERIVATION OF NOZZLE COEFFICIENTS

11.1 Effective Velocity Coefficient

The effective velocity coefficient is defined as the ratio of the effective velocity assuming complete expansion to the isentropic fully expanded velocity or,

$$C_{\text{vf}} = \frac{\frac{F_g}{w_{g/g}}}{(v_f)_{is}} = \frac{v_{\text{eff}}}{(v_f)_{is}} = \frac{\int_{(v_f)_{is}}^{Ae} \left[v_e^2 + (v_e^2 - v_f^2) \right] dA}{(v_f)_{is}}, \qquad (1)$$

where the symbols are defined in Section 9 and the flow stations are given by Figure 28. Use of this equation is as follows:

- a. F_g , W_g , T_{t_d} is measured as a function of nozzle pressure ratio
- b. The isentropic fully expanded velocity is defined as

$$(\mathbf{v_f})_{\mathbf{is}}^2 = \frac{2\mathbf{g} \quad \mathbf{T_{t_d}} \mathbf{v}_R}{\mathbf{v}_{-1}} \left[1 - \left(\frac{\mathbf{v_f}}{\mathbf{v}_{t_d}} \right) \right]$$
(2)

c. Substitution in Equation (1) results as

$$C_{vf} = \sqrt{\frac{2 T_{t_d} \chi R}{g (\chi - 1)} \left[1 - \left(\frac{P_f}{P_{t_d}} \right) \frac{\chi - 1}{\chi} \right]}$$
(3)

Note:
$$\frac{P_f}{P_{t_d}} = \frac{1}{\overline{NPR}}$$

d. For 0 = 1.35 and R = 53.35 #ft/#° R

$$C_{vf} = \frac{0.280 \text{ Fg}}{\sqrt{T_{t_d} \left[1 - \left(\frac{P_f}{P_{t_d}}\right)^{0.259}\right]}}$$
(4)

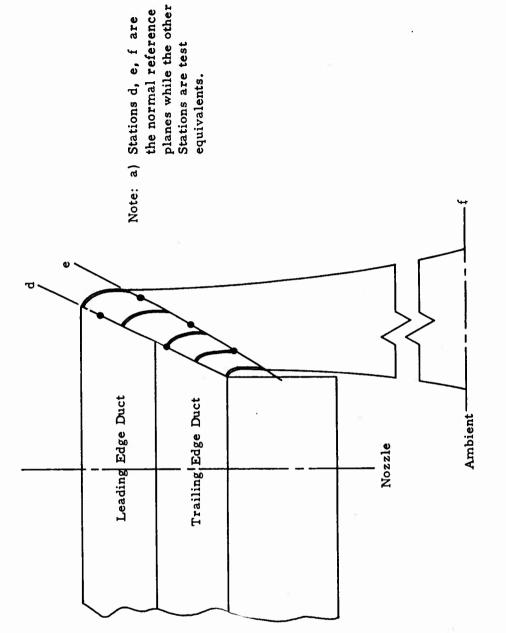


Figure 28. Station Designations for Nozzle Coefficient Derivations

e. For unchoked conditions, an alternate form of the isentropic fully expanded velocity is convenient. Since $(P_f)_{is} = (P_e)_{is}$ for unchoked conditions

$$(v_e)_{is}^2 = \forall g R T_{t_d} (w_e)_{is}^2$$
,

where,

$$\left(\mathbf{M}_{\mathbf{e}}\right)_{\mathbf{is}}^{2} = \frac{2}{X-1} \left[\left(\frac{\mathbf{P}_{\mathbf{td}}}{\mathbf{P}_{\mathbf{f}}}\right) \frac{X-1}{X} - 1 \right].$$

Substituting in Equation (1)

$$C_{\mathbf{v}\,\mathbf{f}} = \frac{\mathbf{F}_{\mathbf{g}}}{\mathbf{V}_{\mathbf{g}}\mathbf{M}_{\mathbf{e}}} \sqrt{\frac{\mathbf{g}}{\mathbf{X}^{\mathbf{R}}\mathbf{T}_{\mathbf{e}}}}.$$
 (5)

Finally, for χ = 1.35 and R = 53.35 ft/f° R

$$C_{vf} = \frac{0.668 F_g}{W_g M_e \sqrt{T_e}}.$$
 (6)

11.2 Thrust Coefficient

The nozzle thrust coefficient is defined as the ratio of actual to ideal thrust or.

$${}^{C}_{f} = \frac{F_{g}}{(F_{g})_{is}} = \frac{\int^{A_{e}} \frac{v_{e} dw_{g}}{g} + (P_{e} - P_{f}) dA}{\left(\frac{w_{g} v_{f}}{g}\right)_{is}}$$
(7)

To establish the variables for Equation (7)

- a. Measure the theoretical exit area $\mathbf{A}_{\mathbf{e}}$ and measure $\mathbf{F}_{\mathbf{g}}$ as a function of nozzle pressure ratio.
- b. For choked conditions, the ideal flow rate based on the measured exit area is

$$(\mathbf{w}_{\mathbf{g}})_{\mathbf{i}\mathbf{s}} = (\mathbf{w}_{\mathbf{g}})_{\mathbf{i}\mathbf{s}}^{*} = P_{\mathbf{t}_{\mathbf{d}}} A_{\mathbf{e}} \sqrt{\frac{\mathbf{g}_{\mathbf{g}}}{\mathbf{g}_{\mathbf{t}_{\mathbf{d}}}}} \left(1 + \frac{\mathbf{g}_{-1}}{2}\right)^{-\frac{\mathbf{g}_{+1}}{2(\mathbf{g}_{-1})}}.$$
 (8)

The isentropic velocity for full expansion is

Employing Equations (8) and (9), the isentropic thrust is then

$$(\mathbf{F}_{\mathbf{g}})_{\mathbf{i}\mathbf{s}} = \left(\frac{\mathbf{w}_{\mathbf{g}} \mathbf{v}_{\mathbf{f}}}{\mathbf{g}}\right)_{\mathbf{i}\mathbf{s}} = \mathbf{P}_{\mathbf{t}_{\mathbf{d}}} \mathbf{A}_{\mathbf{e}} \mathbf{v} \left(1 + \frac{\mathbf{v}_{-1}}{2}\right)^{-\frac{\mathbf{v}_{+1}}{2(\mathbf{v}_{-1})}} \left\{ \frac{2}{\mathbf{v}_{-1}} \left[1 - \left(\frac{\mathbf{P}_{\mathbf{f}}}{\mathbf{P}_{\mathbf{t}_{\mathbf{d}}}}\right)^{\frac{\mathbf{v}_{-1}}{\mathbf{v}}}\right] \right\}^{1/2}$$
 (10)

For X = 1.35, the nozzle thrust coefficient becomes

$$C_{f} = \frac{0.532 \text{ Fg}}{P_{t_{d}} \text{ Ae} \left[1 - \left(\frac{P_{f}}{P_{t_{d}}}\right)^{0.259}\right]^{0.5}}.$$
 (11)

Note: $P_f = P_{amb}$.

c. For unchoked conditions, the ideal flow rate for expansion to ambient conditions is given by

$$(w_g)_{is} = P_{t_d} A_e \sqrt{\frac{\chi_g}{R T_{t_d}}} \left(1 + \frac{\chi_{-1}}{2} M_e^2\right)^{-\frac{\chi_{+1}}{2(\chi_{-1})}}.$$
 (12)

Combining with Equation (9), the ideal thrust is

$$(\mathbf{F}_{\mathbf{g}})_{\mathbf{is}} = \left(\frac{\mathbf{w}_{\mathbf{g}} \mathbf{v}_{\mathbf{f}}}{\mathbf{g}} \right)_{\mathbf{is}} = \mathbf{P}_{\mathbf{t}_{\mathbf{d}}} \mathbf{A}_{\mathbf{e}} \mathbf{v} \left(\mathbf{1} + \frac{\mathbf{v}_{\mathbf{f}} - \mathbf{1}}{2} \mathbf{M}_{\mathbf{e}}^{2} \right) - \frac{\mathbf{v}_{\mathbf{f}} + \mathbf{1}}{2(\mathbf{g} - \mathbf{1})} \left\{ \underbrace{\mathbf{z}}_{\mathbf{f} - \mathbf{1}} \left[\mathbf{1} - \left(\frac{\mathbf{P}_{\mathbf{f}}}{\mathbf{P}_{\mathbf{t}_{\mathbf{d}}}} \right) \frac{\mathbf{v}_{\mathbf{f}} - \mathbf{1}}{\mathbf{v}} \right] \right\}^{1/2}$$
 (13)

and, with Equation (7) for arr = 1.35, the nozzle thrust coefficient becomes



€ 4-ROR4H- D->-0-0Z

(14)

$$C_{f} = \frac{0.31 \, F_{g} \left(1 + 0.175 \, M_{e}\right)_{1s}^{2}}{P_{t_{d}}^{A} e \left[1 - \left(\frac{P_{f}}{P_{t_{d}}}\right)^{0.259}\right]^{0.5}}$$

11.3 Flow Coefficient

The nozzle flow coefficient is defined as the actual to ideal flow or,

$$C_{\mathbf{w}} = \frac{\mathbf{w}_{\mathbf{g}}}{(\mathbf{w}_{\mathbf{g}})_{\mathbf{is}}} = \int_{\mathbf{w}_{\mathbf{g}}}^{\mathbf{A}_{\mathbf{e}}} \int_{\mathbf{w}_{\mathbf{g}}}^{\mathbf{A}_{\mathbf{e}}} . \tag{15}$$

Also,

$$\frac{C_{f}}{C_{vf}} = \frac{\frac{F_{g}}{(F_{g})_{is}}}{\frac{F_{g}}{(V_{f})_{is}}} = \frac{\frac{W_{g}}{g}}{\frac{F_{g}}{(V_{f})_{is}}} = \frac{W_{g}}{(W_{g})_{is}}.$$
(16)

Thus,

$$C_{\overline{W}} = \frac{C_{\overline{f}}}{C_{\overline{Vf}}} . \tag{17}$$

UNCLASSIFIED

UNCLASSIFIED